ภาคผนวก

A. Manuscript

1. Title: Understanding on Absorption and Fluorescence Electronic Transitions of Carbazole-Based Conducting Polymers. Theoretical Chemistry Accounts 2010, 125: 35-44.

2. Title: Effects of the CN and NH_2 Substitutions on the Geometrical and Optical Properties of Model Vinylfluorenes, Based on DFT Calculations. Journal of Molecular Structure: THEOCHEM 2010, 939: 75-81.

3. Title: Absorption and Emission Spectra of Methoxy Substituted Cinnamates Investigated Using the Symmetry-Adapted Cluster Configuration Interaction Method. Journal of Chemical Physics 2009, 131: 224306.

Theor Chem Acc (2010) 125:35–44
DOI 10.1007/s00214-009-0655-4

REGULAR ARTICLE

Understanding on absorption and fluorescence electronic transitions of carbazole-based conducting polymers: TD-DFT approaches

Songwut Suramitr · Wichanee Meeto · Peter Wolschann · Supa Hannongbua

Received: 7 May 2009 / Accepted: 5 October 2009 / Published online: 30 October 2009

Abstract The electronic excitation transitions of carbazole-based oligomers, $(Cz\text{-}co\text{-}Cz)_N$, $(Cz\text{-}co\text{-}Fl)_N$ and $(Cz\text{-}co\text{-}Th)_N$ ($N = 2$–4) were investigated using density functional theory (DFT) and time-dependent (TD) DFT methods. Our results show that the calculated ground state geometries favor a more aromatic, planer structure, while the electronically excited geometries favor a quinoidic type structure. Absorption and fluorescence energies have been obtained from TD-B3LYP/SVP calculations performed on the S_1 optimized geometries and are in excellent agreement with experimental data. The experimental fluorescence excitation energies for $(Cz\text{-}co\text{-}Cz)_4$, $(Cz\text{-}co\text{-}Fl)_4$ and $(Cz\text{-}co\text{-}Th)_4$ (2.76, 2.63, and 2.25 eV, respectively) correspond closely with the predicted S_1 transitions (2.84, 3.91 and 2.43 eV, respectively). We also report the predicted radiative lifetimes 0.52, 0.47, and 0.99 ns for $(Cz\text{-}co\text{-}Cz)_N$, $(Cz\text{-}co\text{-}Fl)_N$ and $(Cz\text{-}co\text{-}Th)_N$, discuss the origin of the small stoke shift of the carbazole based oligomers and the magnitude of bathochromic shifts. We conclude by discussing the benefits of theoretical calculations, which can provide critical structural and electronic understanding of excitation–relaxation phenomena that can be exploited in design of novel optical materials.

Keywords Carbazole-based · Density functional theory · TDDFT · Radiative lifetimes

1 Introduction

Conducting polymers as light-emitting diodes, field effect transistors, charge storage devices, photodiodes, sensors, etc. [1, 2] are currently of interest. In the last year, novel well-defined 2,7-carbazole-based (Cz) polymers were synthesized by Leclerc et al. [2–7]. 2,7-Carbazole-based polymers and derivatives with thiophene, pyrrole, phenylene, and fluorene subunits have been synthesised [8–10], are currently of both industrial and academic interest because of their wide-ranging potential in electronic devices. These novel polymeric materials are stable in air and soluble in many usual organic solvents. Interestingly, the absorption and fluorescence spectra of these materials exhibit significant differences [11–13]. It is found that the existence of multi-components in the fluorescence decay profiles of such polymers in the solid state is caused by several distinct intermolecular π–π^* interactions. However, these interactions are not strong enough to provoke the appearance of distinct fluorescence bands or even to increase the bandwidths of the emission bands in solution. Fundamental understanding on structural and energetic properties of this kind of copolymers could lead to beneficial knowledge for the design of novel copolymers. Therefore, it is of interest to compare the absorption and fluorescence transitions of 2,7-carbazole-based polymers and its dependence on the structural and the electronic properties. We are also interested in exploring the

S. Suramitr · W. Meeto · S. Hannongbua
Department of Chemistry, Faculty of Science,
Kasetsart University, Bangkok 10900, Thailand
e-mail: fscisph@ku.ac.th

S. Suramitr (✉) · W. Meeto · S. Hannongbua
The Center of Nanoscience, Kasetsart University,
Bangkok, 10900, Thailand
e-mail: fsciswsm@ku.ac.th

P. Wolschann
Institute for Theoretical Chemistry, University of Vienna,
Währinger Straße 17, 1090 Vienna, Austria

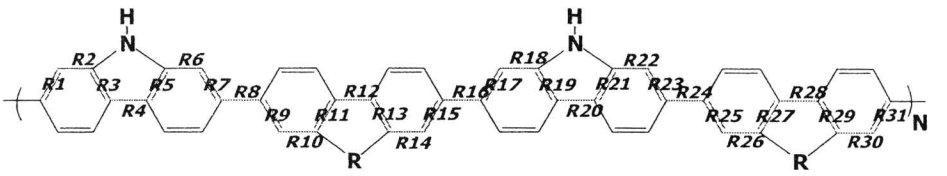

(a) R=NH: -(Cz-co-Cz)$_N$- and R=CH_2: -(Cz-co-Fl)$_N$-

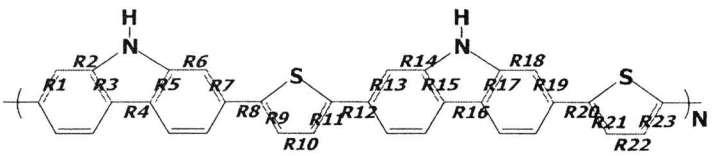

(b) -(Cz-co-Th)$_N$-

Fig. 1 Structures and numbering schemes of **a** (Cz-co-Cz)$_N$ and (Cz-co-Fl)$_N$ and **b** (Cz-co-Th)$_N$ oligomers

excitation mechanism since this will affect the pattern of the emission bands.

In previous studies of carbazole-based molecules [11–13], calculations were performed using DFT as well as (TD-DFT) with the B3LYP functional and three basis sets: 6-31G, 6-31G(*d*) and 6-311G(*d*,*p*). However, only ground state conformational analysis and calculations of the vertical excitation energies were carried out. From these calculations, it was reported that the optimized ground state geometries of oligomers with six-membered heterocyclic rings copolymers are nonplanar, whereas planar copolymer structures were found for with five-membered heterocyclic ring a results of the subtle balance between minimizing steric repulsion and maximizing electronic conjugation [14].

To increase our understanding of this important polymer class, we have performed calculations on the excited state properties of carbazole-based homopolymers and copolymers with fluorene and thiophene substituents (formulas are given in Fig. 1). In this study, we put particular emphasis on understanding the ground and low-lying excited states of the carbazole-homopolymer (Cz-co-Cz)$_N$, carbazole-co-fluorene (Cz-co-Fl)$_N$ and carbazole-co-thiophene (Cz-co-Th)$_N$ oligomers, which are explored by theoretical studies. The transitions associated with the absorption and fluorescence spectra of carbazole-based oligomers are explored. The fluorescence energies and radiative lifetimes are also analyzed in an attempt to gain better, more general understanding of the behavior of such systems.

2 Computational details

All QM calculations were performed using TURBOMOLE version 5.7 [15]. All geometry optimizations were performed using TURBOMOLE's JOBEX program with generalized internal coordinates and the corresponding STATPT module [16]. The ground state and the lowest singlet excited-state geometries of the carbazole-based oligomers were optimized by DFT and TDDFT, respectively, using the B3LYP [17–21] functional for the carbazole homopolymer (Cz-co-Cz)$_N$, the carbazole-co-fluorene (Cz-co-Fl)$_N$ and the carbazole-co-thiophene (Cz-co-Th)$_N$ oligomers (Fig. 1). The default m^3 numerical quadrature grid [22] was employed in all DFT calculations. The geometries of carbazole-based analogs were optimized without symmetry constraints using redundant internal coordinates and were considered converged if the gradient was less than 10^{-4} au. In all optimizations, the criterion for convergence was set to 10^{-8} for the energy and 10^{-7} for the density. To calculate excitation energies and analytic excited-state gradients, the TD-DFT method was used. Modules DSCF [22], GRAD, and ESCF [23] have been used. Sufficiently converged results were obtained with the valence-double-zeta quality with polarization functions SVP basis sets in close agreement with many previous studies; the conclusions are thus not expected to vary upon further basis set extensions [11–13]. In order to consider solvent effects on excitation energies, we adopted the conductor-like screening model (COSMO) [24] with a dielectric constant of $\varepsilon = 4.8$ to simulate the chloroform solvent and optimized atomic radii (C, 2.00 Å; N, 1.83 Å; O, 1.72 Å; H, 1.30 Å) for the construction of the molecular cavity were used for the calculations of all molecules.

For each oligomer in Fig. 1, the chain lengths studied varied from dimers to tetramers ($N = 1$, 2, 3 and 4). The first five singlet–singlet electronic transitions ($S_0 \rightarrow S_n$) were calculated for (Cz-co-Cz)$_N$, (Cz-co-Fl)$_N$, and (Cz-co-Th)$_N$ oligomers using the B3LYP/SVP and TD-B3LYP/SVP methods, respectively. Based on the optimized geometries of the oligomers, the electronic absorption and fluorescence spectra were calculated at the DFT and TD-DFT levels. The absorption and fluorescence excitation energies were obtained from the ground state and the

Table 1 Bond torsional angles of oligomers in ground (S_0) and lowest excited state (S_1) (in brackets) for the $(Cz\text{-}co\text{-}Cz)_N$, $(Cz\text{-}co\text{-}Fl)_N$ and $(Cz\text{-}co\text{-}Th)_N$ molecules optimized using B3LYP/SVP and TD-B3LYP/SVP (in parenthesis) methods

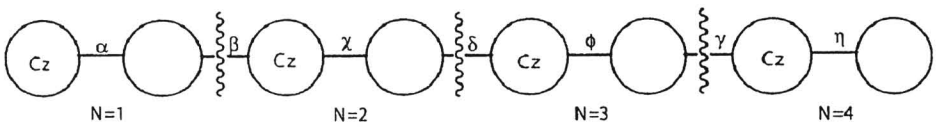

Oligomers	Bond torsional angles (°)						
	α	β	χ	δ	ϕ	γ	η
$(Cz\text{-}co\text{-}Cz)_N$							
$N = 1$	140.51						
	(170.24)						
$N = 2$	141.54	141.15	141.56				
	(155.15)	*(163.88)*	*(155.03)*				
$N = 3$	141.94	142.79	142.80	142.76	142.00		
	(147.13)	*(155.54)*	*(160.24)*	*(155.39)*	*(146.68)*		
$N = 4$	141.99	141.58	142.25	143.44	141.88	141.77	141.91
	(146.06)	*(152.82)*	*(159.91)*	*(154.50)*	*(155.69)*	*(148.60)*	*(143.88)*
$(Cz\text{-}co\text{-}Fl)_N$							
$N = 1$	142.14						
	(170.71)						
$N = 2$	142.20	142.19	142.30				
	(156.46)	*(167.58)*	*(155.39)*				
$N = 3$	142.53	143.38	142.40	143.21	142.42		
	(146.86)	*(157.03)*	*(164.52)*	*(157.34)*	*(148.24)*		
$N = 4$	142.69	142.60	142.44	141.78	142.66	142.59	143.04
	(156.46)	*(167.58)*	*(155.39)*	*(167.58)*	*(156.46)*	*(167.58)*	*(155.39)*
$(Cz\text{-}co\text{-}Th)_N$							
$N = 1$	21.06						
	(0.01)						
$N = 2$	27.23	27.41	27.00				
	(0.02)	*(0.00)*	*(0.00)*				
$N = 3$	24.19	24.52	25.67	24.72	25.61		
	(0.02)	*(0.04)*	*(0.02)*	*(0.00)*	*(0.03)*		
$N = 4$	26.82	25.78	27.81	26.14	27.53	25.49	26.04
	(0.00)	*(0.01)*	*(0.01)*	*(0.00)*	*(0.01)*	*(0.00)*	*(0.02)*

All torsional angles are given in degrees. N represents the number of the oligomer units

lowest singlet excited-state optimized geometries. The fluorescence electronic transitions were calculated as the vertical de-excitation based on the optimized geometry of the lowest excited state.

3 Results and discussion

3.1 Ground and excited states structural properties

The chain length dependence on the oligomer torsional angles (θ), both at ground and excited state has been investigated for the carbazole-based oligomers using our ground state optimized geometries. The torsion angles of the oligomers are given in Table 1 for the ground (S_0) and the lowest excited state (S_1) for the $(Cz\text{-}co\text{-}Cz)_N$, $(Cz\text{-}co\text{-}Fl)_N$ and $(Cz\text{-}co\text{-}Th)_N$ molecules.

The optimized structures of carbazole-based oligomers in the ground states are generally more distorted than the structures in excited states. We found twisted conformations with torsional angles (α, β, χ, δ, ϕ, γ and η) around 140° for both Cz-co-Cz-co-Cz and Cz-co-Fl-co-Cz. For Cz-co-Th-co-Cz, the torsional angles are around 30°, which means that the *syn* or *cis* structure of the copolymerized

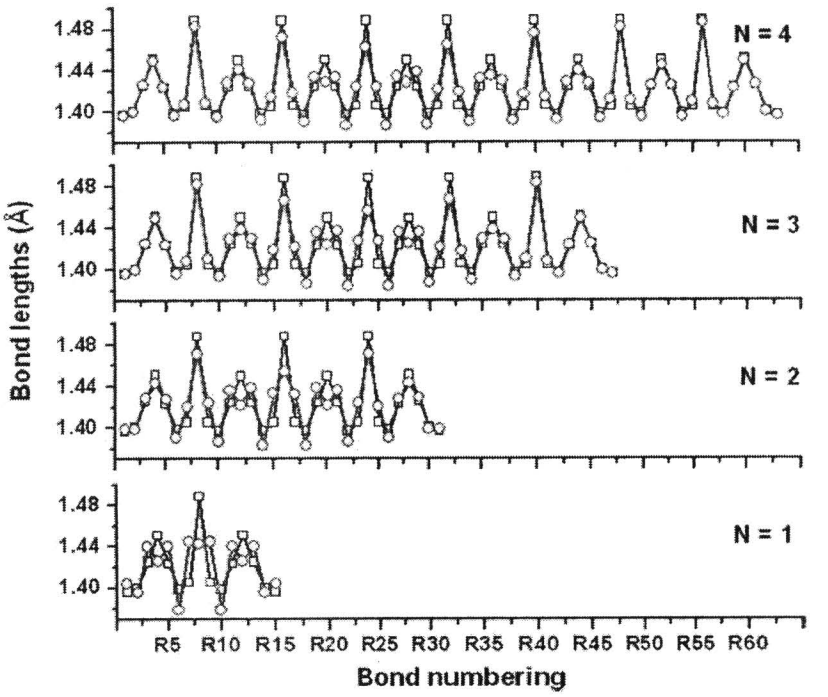

Fig. 2 Computed bond lengths of ground state and excited state of homocarbazole oligomers (Cz-co-Cz)$_N$. The *open square* denote electronic ground state and the *open circle* indicate the first excited state. Calculated at the B3LYP/SVP level of theory

heterocycles ring (thiophene) is energetically more favorable than the "trans" conformations [11, 12].

These ground state torsional angles appear independent the number of oligmer subunits used in the calculations. Only in the case of (Cz-co-Th)$_N$ is the monomer more planar than the oligomers. On the contrary, the excited state-torsion angles are more planar than the ground state geometries with torsional angles around 180° or 0°, respectively. The differences in the bond torsional angles between the ground and lowest singlet excited state can be explained by considering the bond length changes. The structures of the ground state and the lowest singlet excited-state optimized oligomers geometries are given in Figs. 2 and 3, where the changes bond lengths for copolymer derivatives and carbazole-based oligomer can be compared. The bond numbering schemes of (Cz-co-Cz)$_N$, (Cz-co-Fl)$_N$ and (Cz-co-Th)$_N$ oligomers are depicted in Fig. 1. In Fig. 2, the conjugated carbon–carbon bonds are illustrated for the ground state (S_0) and singlet excitations (S_1) for (Cz-co-Cz)$_N$ oligomers, dimer to octamer.

From Fig. 2, it is found that the carbon–carbon bonds which lie parallel to the polymer chain (i.e. bond numbering *R2*, *R4*, *R6*, *R8*, *R10*, *R12* and *R14*) become shorter while those that lie at angles other than 180° become longer. The carbon–carbon bonds are found to alternate in length between a single and double bond. In the lowest excited states, the double bond lengths increase, whereas the single bond length decreases with the changes being localized toward the centre of the oligomers. For example, the geometric changes in (Cz-co-Cz)$_1$, (Cz-co-Cz)$_2$, (Cz-co-Cz)$_3$ and (Cz-co-Cz)$_4$ due to excitation affect the central units only. It should be noted that the spatial extent of the geometry deformations is not constant; the deformations continue to extend over the entire chain when the length increases, at least up to (Cz-co-Cz)$_{N=4}$ and this can be understood in terms of the degree of charge delocalization. For longer chains, the amount of charge per monomer unit is lower and thus the geometry change is smaller. The geometry change, as obtained from DFT calculations, are found in all the (Cz-co-Cz)$_N$ oligomer chains. This suggests that the center rings in the larger carbazole-based oligomers have more quinoidic character than the terminal rings [12, 13]. Therefore, the central rings in the larger oligomers were selected to confirm the trends of the C–C bond alternation along the backbone of the (Cz-co-Cz)$_3$, (Cz-co-Fl)$_3$ and (Cz-co-Th)$_3$ as shown in Fig. 3. We monitor the changes in bond length of these aromatic systems using the bond length alternation (BLA) [25]. The BLA values for selected molecular fragment can be defined as the differences in lengths between single bonds (d_{single}) and double bonds (d_{double}) of carbon–carbon atoms (Eq. 1). A positive BLA value indicates that the molecular unit has an aromatic (quinoidic) character [26–28].

$$BLA = \sum \frac{(d_{\text{single}} - d_{\text{double}})}{N}, \tag{1}$$

The BLA associated with the carbon–carbon conjugated bond for the ground and singlet excitations states for the central rings of (Cz-co-Cz)$_3$, (Cz-co-Fl)$_3$ and (Cz-co-Th)$_3$ oligomer was estimated. We find that the BLA changes

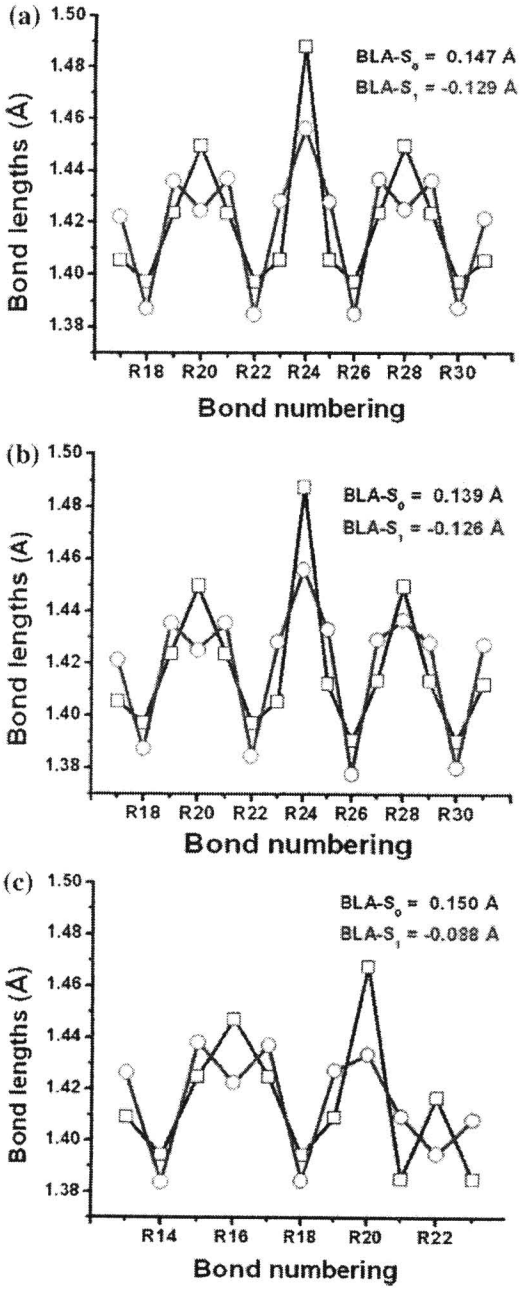

Fig. 3 The bond length alternating (BLA) of the central rings of the oligomers of (**a**) $(Cz\text{-}co\text{-}Cz)_3$, (**b**) $(Cz\text{-}co\text{-}Fl)_3$ and (**c**) $(Cz\text{-}co\text{-}Th)_3$ as shown. The open square denote electronic ground state and the open circle indicate the first excited state. Calculated using TD-DFT at the B3LYP/SVP level of theory

significantly in the excited states compared to the ground states, in the case of $(Cz\text{-}co\text{-}Cz)_3$ and $(Cz\text{-}co\text{-}Fl)_3$, decreasing from 0.147, 0.139 Å in S_0 to −0.129, −0.125 Å in S_1, respectively. In both, the ground and singlet states, the BLA differences are between 0.014 and 0.019 Å, whereas in the case of $(Cz\text{-}co\text{-}Th)_3$, the BLA decreases from 0.150 Å in S_0 to −0.088 Å in S_1. These results indicate that the thiophene unit leads to a decrease in the BLA value by 0.063 Å with respect to the $(Cz\text{-}co\text{-}Cz)_3$ and $(Cz\text{-}co\text{-}Fl)_3$ oligomers. In addition, the center of the quinoidic structures is located at the linking bonds between the copolymer units such as *R8*, as seen clearly in Fig. 1. Chidthong et al. [29] and Wichanee et al. [13] suggest that the elongation of the molecular chain leads to minor changes in the inter-ring distances of oligomers, the largest change localized at the terminal ring. In addition to, it was found that the inter-ring bond distances do not display appreciable variations with the oligomer size. Moreover, the bond-changing pattern is varied systematically when the molecular chain is elongated. These behaviors have been also found in the case of carbazole-based homopolymer and copolymer oligomers.

3.2 Absorption and fluorescence transitions

The absorption and fluorescence excitation energies calculated by the TD-B3LYP/SVP method are reported in Table 2. The excitations energies with highest oscillator strength (π–π^* transition) of each polymer calculated by TD-B3LYP/SVP method and were extrapolated by linear regression. There is a good linear relation ($r^2 = 0.99$) between the lowest excitations and the inverse chain length. A comparison the extrapolated energy of the absorption and fluorescence excitation with the experimental results and other computed values is shown in Table 2. From these results, it was found that the excitation energies of these materials are lower than the experimental data, 0.34, 0.31, and 0.18 eV (absorption) and 0.33, 0.51, and 0.69 eV (fluorescence) for its carbazole-based, $(Cz\text{-}co\text{-}Cz)_N$, $(Cz\text{-}co\text{-}Fl)_N$ and $(Cz\text{-}co\text{-}Th)_N$, respectively. Cornil et al. [30, 31] have shown that this can result from the overestimation of long-range electron correlation effects in the TD-DFT methods. Previous works [30–33] have shown that the high accuracy of DFT functionals such as TPSS functional is more suitable for calculation of conjugated oligomers. However, for small molecules, the impact of inductive and/or mesomeric effects induced by substituents appears to be well reproduced; however, the agreement with the correspondingly experimental values deteriorates when the chain size is increased. Our results confirm previous reports that a proper extrapolation procedure recommends the use of a rather large number of oligomers to improve the accuracy of the fit, and an accurate fitting function [30, 31, 34–37]. In fact, in order to obtain more accurate excitation energy for an infinite oligomer, one needs to use higher order polynomials. Jansson et al. studied the chain length dependence of singlet and triplet excited states of oligofluorene and used an empirical relationship proposed by Meier et al. [35, 36]. They discussed in detail the concept of "effective conjugation length"

Table 2 The calculation absorption (E_{abs}), fluorescence energies (E_{flu}) and fluorescence lifetimes of carbazole-based polymers

Oligomers	Absorption	Fluorescence	
	E_{abs} (eV)	E_{flu} (eV)	Lifetime (ns)
$(Cz\text{-}co\text{-}Cz)_N$			
$N = 1.0$	3.84	3.28 (1.484)	1.44
$N = 1.5$	3.51	2.91 (2.482)	1.10
$N = 2.0$	3.36	2.83 (3.222)	0.89
$N = 2.5$	3.26	2.77 (3.933)	0.76
$N = 3.0$	3.21	2.76 (4.561)	0.66
$N = 4.0$	3.17	2.76 (5.814)	0.52
$N = \infty$	2.91	2.51	
Expt.	3.25[a]	2.84[a]	
$(Cz\text{-}co\text{-}Fl)_N$			
$N = 1.0$	3.80	3.23 (1.517)	1.46
$N = 2.0$	3.32	2.77 (3.242)	0.93
$N = 3.0$	3.18	2.68 (4.537)	0.71
$N = 4.0$	3.14	2.63 (7.076)	0.47
$N = \infty$	2.89	2.40	
Expt.	3.20[a]	2.91[a]	
$(Cz\text{-}co\text{-}Th)_N$			
$N = 1.0$	3.87	3.59 (0.862)	2.07
$N = 2.0$	3.14	2.57 (2.318)	1.50
$N = 3.0$	2.87	2.34 (3.517)	1.20
$N = 4.0$	2.81	2.25 (4.598)	0.99
$N = \infty$	2.42	1.74	
Expt.	2.60[b]	2.43[b]	

Values in parentheses are oscillator strengths

[a] Ref. [6]

[b] Ref. [7]

(ECL), defined as the conjugation length at which the wavelength of the absorption maximum in the series of oligomers is not more than 1 nm above the lower limit, which is given by the infinitely long polymer chain [30, 35–37]. From this definition, the ECL largely differs for the various oligomer series. Given these issues, we focus on ECL for estimate the excitation energies of these systems in the following section.

We estimate the ECL for all selected oligomers based on the convergence of the calculated excited energies of the first dipole-allowed excited states with the increasing chain length (Fig. 4). The ECL was estimated by the convergence of excitation energies with the chain length within a threshold of 0.05 eV, based on the obtained linearity between the excitation energy and reciprocal chain length. Apart from the selected carbazole-based oligomers, well-studied oligomers, such as $(Cz\text{-}co\text{-}Cz)_N$, $(Cz\text{-}co\text{-}Fl)_N$ and $(Cz\text{-}co\text{-}Th)_N$ oligomers are also reexamined with TDDFT for further validating the theory and for comparison. These results will be discussed only briefly.

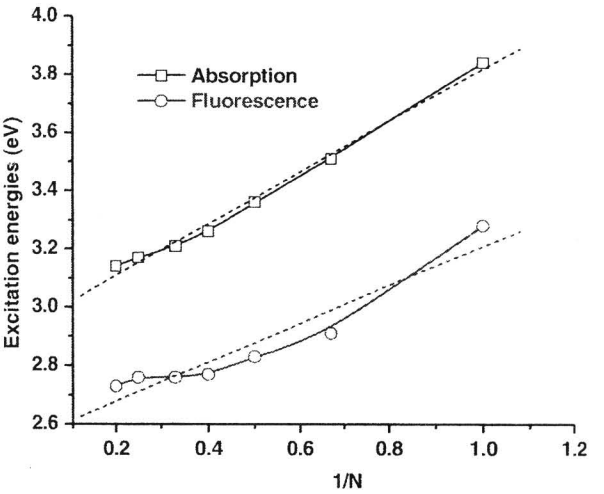

Fig. 4 First singlet excitation energies as calculated by TDDFT for absorption and fluorescence energies in poly(2,7-carbazole) oligomers, as a function of $1/N$

We present their absorption and fluorescence energies in Table 2 by applying the ECLs for the absorption and fluorescence energies for compounds $(Cz\text{-}co\text{-}Cz)_N$, $(Cz\text{-}co\text{-}Fl)_N$ and $(Cz\text{-}co\text{-}Th)_N$ oligomers. The ECL value at which a convergence of the optical properties, absorption and emission properties is reached corresponds to $N = 4$ for $(Cz\text{-}co\text{-}Cz)_N$, $(Cz\text{-}co\text{-}Fl)_N$ and $(Cz\text{-}co\text{-}Th)_N$ oligomers. Comparison of the results between experiment and absorption spectrum calculations of are shown in Fig. 5 and indicate that the estimated excitation energies, at ECLs $N = 4$, are in good agreement with the optical properties. We therefore conclude that this procedure can be used to reliably estimate the excitation energies of such polymers.

We next look at the details of the electronic transitions of each carbazole-based tetramer ($N = 4$) at TD-B3LYP/SVP level (Table 3) which can be used to describe the possible excitations of all carbazole-based molecules. From the absorption transitions, it was found that for $(Cz\text{-}co\text{-}Cz)_4$, $(Cz\text{-}co\text{-}Fl)_4$ and $(Cz\text{-}co\text{-}Th)_4$ molecules, the $S_0 \rightarrow S_1$ excitation primarily corresponds to the promotion of an electron from the highest occupied molecular orbital (HOMO) to the lowest unoccupied molecular orbital (LUMO) (H → L) (in Fig. 6) as indicated by large oscillator strengths (f) of : 6.112, 6.169 and 4.277, respectively. The isosurface plot of the HOMO and LUMO (Fig. 6) indicate an exchange of the double and single bonds as is typical for a $\pi \rightarrow \pi^*$ transition in conjugated polymers. On the other hand, the S_2, S_3 and S_4 electronic transitions of each compound possess very small oscillator strengths. The fluorescence energies and the radiative lifetimes of $(Cz\text{-}co\text{-}Cz)_4$, $(Cz\text{-}co\text{-}Fl)_4$ and $(Cz\text{-}co\text{-}Th)_4$ computed with the TD-B3LYP/SVP method using S_1 state optimized geometries are collected in Table 3. The fluorescence energies were

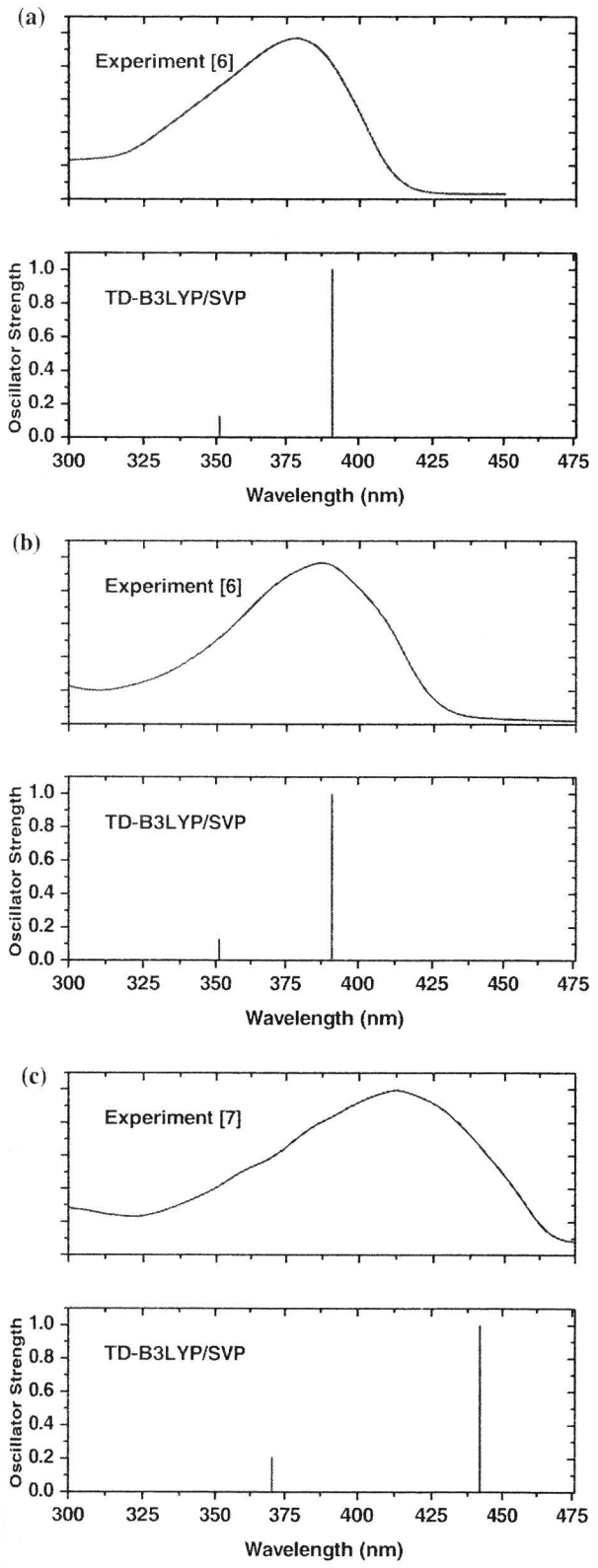

Fig. 5 Absorption spectra [6, 7] and TD-B3LYP/SVP calculations of $(Cz\text{-}co\text{-}Cz)_4$, $(Cz\text{-}co\text{-}Fl)_4$ and $(Cz\text{-}co\text{-}Th)_4$ oligomers

also investigated. From Table 2, it is clear that the fluorescence energies of $(Cz\text{-}co\text{-}Th)_N$ and $(Cz\text{-}co\text{-}Fl)_N$ molecules are red-shifted from the excitation energies of $(Cz\text{-}co\text{-}Cz)_N$ with values of 2.76, 2.63 and 2.25 eV for $(Cz\text{-}co\text{-}Cz)_N$, $(Cz\text{-}co\text{-}Fl)_N$ and $(Cz\text{-}co\text{-}Th)_N$, respectively. These energies are in good agreement with experimental values [6, 7].

The differences in absorption and fluorescence energies should also lead to different Stokes shifts. We therefore evaluate the Stokes-shift as the differences $\Delta E = E_{abs} - E_{flu}$. The TD-B3LYP/SVP values exhibit Stokes shift of about 0.3 eV for $(Cz\text{-}co\text{-}Fl)_N$ and are lower than those for $(Cz\text{-}co\text{-}Cz)_N$ and $(Cz\text{-}co\text{-}Th)_N$ by about 0.6 eV. This result demonstrates that the $(Cz\text{-}co\text{-}Fl)_N$ structure is more relaxed than those of $(Cz\text{-}co\text{-}Cz)_N$ and $(Cz\text{-}co\text{-}Th)_N$ upon excitation. These results also show that the electronic excitation leads to the formation of a quinoide-type structure.

Using the computed structures, we can also relate the differences in the bond lengths between the ground (GS) and lowest singlet excited state (ES) to the molecular orbital nodal patterns. Because the lowest singlet state corresponds to an excitation from the HOMO to the LUMO in all of the oligomers considered here (Fig. 5), the bond-length variations were explored further in terms of the changes to the HOMO and LUMO. By comparing Fig. 5, we can see that the HOMO has nodes across the *R1, R3, R5, R7, R9, R11* and *R13* bonds in all molecules, but the LUMO is bonding in these regions. Therefore, one would expect a contraction of these bonds. The data reported in Fig. 2 and Fig. 3 do in fact show this given the bonds are in fact considerably shorter in the excited state. However, the bond length will increase when the bonding changes to antibonding. The dihedral angle (Table 1) between the two adjacent units shortened from 140° to 170° in $(Cz\text{-}co\text{-}Cz)_N$ and $(Cz\text{-}co\text{-}Fl)_N$ molecules. Whereas the dihedral angle of $(Cz\text{-}co\text{-}Th)_N$ shortened from 28° to nearly 0°. It is obvious that the excited structure has a strong coplanar tendency in all molecules. It is indicated that is, the conjugation is better in the excited structure. In this result, it can see that geometry of excited state is more planar than ground state.

Finally, to investigate the effects of the structural relaxation upon excitation, radiative lifetimes were investigated. Based on the fluorescence energy and oscillator strength, the radiative lifetimes have been computed for spontaneous emission using the Einstein transition probabilities according to the formula (in au) [29, 38, 39].

$$\tau = \frac{c^3}{2(E_{Flu})^2 f} \tag{2}$$

In Eq. 2, c is the velocity of light, E_{Flu} is the transition energy and f is the oscillator strength. The computed lifetimes, τ, for the carbazole-based oligomers are depicted

Table 3 Excitation energies (E_{ex}(eV)), oscillator strengths (f), and wave function compositions for the lowest singlet electronic states of (Cz-co-Cz)$_4$, (Cz-co-Fl)$_4$ and (Cz-co-Th)$_4$ molecules computed by TD-B3LYP/SVP

Electronic transitions	E_{ex}	f	Wave function composition
(Cz-co-Cz)$_4$			
Absorption			
$S_0 \rightarrow S_1$	3.17	6.112	H → L(61.8%), H-1 → L+1(25.1%)
$S_0 \rightarrow S_2$	3.34	0.002	H-1 → L(45.8%), H → L+1(45.8%)
$S_0 \rightarrow S_3$	3.51	0.773	H-1 → L+1(46.5%), H → L+2(31.8%)
$S_0 \rightarrow S_4$	3.54	0.008	H-1 → L+1(47.4%), H → L+1(46.8%)
Fluorescence			
$S_1 \rightarrow S_0$	2.76	5.814	H → L(65.3%), H-1 → L+1(17.8%)
(Cz-co-Fl)$_4$			
Absorption			
$S_0 \rightarrow S_1$	3.14	6.169	H → L(61.4%), H-1 → L+1(25.8%)
$S_0 \rightarrow S_2$	3.31	0.011	H-1 → L(46.4%), H → L+1(45.4%)
$S_0 \rightarrow S_3$	3.50	0.039	H → L+1(46.9%), H-1 → L(46.3%)
$S_0 \rightarrow S_4$	3.51	0.731	H → L+1(47.1%), H-2 → L(30.6%)
Fluorescence			
$S_1 \rightarrow S_0$	2.63	7.076	H → L(59.9%), H + 1→L + 1(28.7%)
(Cz-co-Th)$_4$			
Absorption			
$S_0 \rightarrow S_1$	2.81	4.277	H → L(65.0%), H-1 → L+1(18.4%)
$S_0 \rightarrow S_2$	3.10	0.000	H → L+1(47.9%), H-1 → L (45.3%)
$S_0 \rightarrow S_3$	3.18	0.012	H-1 → L+1(50.0%), H → L+1(47.0%)
$S_3 \rightarrow S_4$	3.35	0.886	H-1 → L+1(63.3%), H → L (19.1%)
Fluorescence			
$S_1 \rightarrow S_0$	2.25	4.598	H → L(65.7%), H-1 → L+1(13.3%)

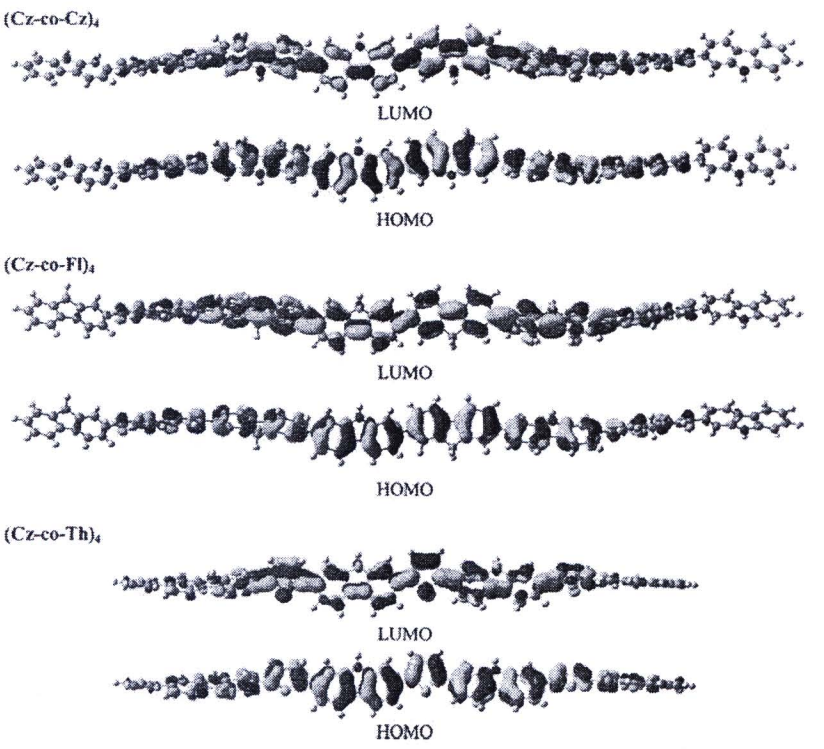

Fig. 6 HOMO and LUMO of (Cz-co-Cz)$_4$, (Cz-co-Fl)$_4$ and (Cz-co-Th)$_4$ oligomers. Depicted are two isosurfaces of equal values but opposite sign

in Table 2. The lifetime of carbazole-based oligomers at $N = 4$ amounts to 0.52, 0.47, and 0.99 ns for $(Cz\text{-}co\text{-}Cz)_N$, $(Cz\text{-}co\text{-}Fl)_N$ and $(Cz\text{-}co\text{-}Th)_N$, respectively. Among the carbazole-based molecules, the $(Cz\text{-}co\text{-}Fl)_N$ shows the lowest lifetime, which is close to that of $(Cz\text{-}co\text{-}Cz)_N$. For the purpose of comparison, the results of a chemically similar system were used. The radiative lifetimes of poly(*N*-octyl-2,7-carbazole) and poly(*N*-octyl-2,7-carbazole-alt-9,9-dioctyl-2,7-fluorene) in THF solution are 0.51 and 0.45 ns [28] which is in good agreement with the predicted lifetimes of $(Cz\text{-}co\text{-}Cz)_N$ (0.52 ns) and $(Cz\text{-}co\text{-}Fl)_N$ (0.47 ns), respectively. Similar results have been reported for several other polymers (thin films) [40–44] and it can be concluded that their low radiative lifetime can produce useful fluorescent emission [40–44].

4 Conclusions

Absorption and fluorescence properties of $(Cz\text{-}co\text{-}Cz)_N$, $(Cz\text{-}co\text{-}Fl)_N$ and $(Cz\text{-}co\text{-}Th)_N$, are presented herein. The optimized ground state and the first singlet excited electronic state have been obtained using B3LYP and TD-B3LYP, methods, respectively, in conjunction with the SVP basis set. A chloroform solvent effect on excitation has been assessed using the COSMO implicit solvent model.

The estimated excitation energies of the absorption and fluorescence excitation based on ECLs $N = 4$ are in good agreement with the optical properties of $(Cz\text{-}co\text{-}Cz)_N$, $(Cz\text{-}co\text{-}Fl)_N$ and $(Cz\text{-}co\text{-}Th)_N$ polymers, 3.17, 3.14 and 2.81 eV (absorption) and 2.76, 2.63 and 2.25 eV (fluorescence), respectively. Compared to experimental fluorescence excitation energies available for $(Cz\text{-}co\text{-}Cz)_N$, $(Cz\text{-}co\text{-}Fl)_N$ and $(Cz\text{-}co\text{-}Th)_N$, it can be seen that TD-B3LYP/SVP calculations give good predictions of the excitation energies for the S_1 transition (2.84, 2.91 and 2.43 eV, respectively). This suggests that the procedure used herein is reliable method for the estimation of excitation energies of such polymers.

Moreover, we find that the geometry of excited states is more planar than that of the ground states. The excitation to the S_1 state causes significant changes in the predicted geometry which is in agreement with the small Stokes shifts observed experimentally. Furthermore, the radiative lifetime of carbazole-based oligomers at $N = 4$ amounts to 0.52, 0.47 and 0.99 ns for $(Cz\text{-}co\text{-}Cz)_N$, $(Cz\text{-}co\text{-}Fl)_N$ and $(Cz\text{-}co\text{-}Th)_N$, respectively, which is in agreement with the experiment lifetimes of $(Cz\text{-}co\text{-}Cz)_N$ (0.51 ns) and $(Cz\text{-}co\text{-}Fl)_N$ (0.45 ns), respectively. It is shown that the existence of multi-components in the fluorescence decay profiles of polymers is caused by several distinct intermolecular π–π^* interactions. We therefore conclude that homopolymers and copolymers derived from *N*-substituted-2,7-carbazoles appear to be very promising materials for the future development of light-emitting diodes, electrochromic windows, photovoltaic cells, photorefractive materials.

Acknowledgments Supporting from the Thailand Research Fund (RTA5080005 to SH and MRG5180287 to SS), and the National Center of Excellence in Petroleum, Petrochemical Technology, Center of Nanotechnology Kasetsart University, Kasetsart University Research and Development Institute (KURDI), National Nanotechnology Center (NANOTEC) and Laboratory of Computational and Applied Chemistry (LCAC) are gratefully acknowledged. The calculations were performed in part on the Schrödinger III cluster of the University of Vienna. Thanks are also due to Matthew Paul Gleeson for helpful comments and reading of the manuscript.

References

1. Burroughes JH, Bradley DDC, Brown AR, Marks RN, Friend RH, Burn PL, Holmes AB (1990) Light-emitting diodes based on conjugated polymers. Nature 347:339–341
2. Morin JF, Beaupre S, Leclerc M, Levesque I, D'Iorio M (2002) Blue light-emitting devices from new conjugated poly(*N*-substituted-2,7-carbazole) derivatives. Appl Phys Lett 80(3):341–343
3. Morin JF, Leclerc M (2001) Syntheses of conjugated polymers derived from *N*-alkyl-2,7-carbazoles. Macromolecules 34(14): 4680–4682
4. Zotti G, Schiavon G, Zecchin S, Morin JF, Leclerc M (2002) Electrochemical, conductive, and magnetic properties of 2,7-carbazole-based conjugated polymers. Macromolecules 35(6): 2122–2128
5. Morin JF, Boudreault PL, Leclerc M (2003) Blue-light-emitting conjugated polymers derived from 2,7-carbazoles. Macromol Rapid Commun 23:1032–1036
6. Bouchard J, Belletete M, Durocher G, Leclerc M (2003) Solvatochromic properties of 2,7-carbazole-based conjugated polymers. Macromolecules 36:4624–4630
7. Morin JF, Leclerc M (2002) 2,7-Carbazole-based conjugated polymers for blue, green, and red light emission. Macromolecules 35(22):8413–8417
8. Belletete M, Bedard M, Leclerc M, Durocher G (2004) Absorption and emission properties of carbazole-based dyads studied from experimental and theoretical investigations. Synth Met 146(1):99–108
9. Belletete M, Bedard M, Leclerc M, Durocher G (2004) Ground and excited state properties of carbazole-based dyads: correlation with their respective absorption and fluorescence spectra. J Mol Struct (THEOCHEM) 679(1–2):9–15
10. Belletete M, Bedard M, Bouchard J, Leclerc M, Durocher G (2004) Spectroscopic and photophysical properties of carbazole-based triads. J Can J Chem 82:1280–1288
11. Suramitr S, Hannongbua S, Wolschann P (2007) Conformational analysis and electronic transition of carbazole-based oligomers as explained by density functional theory. J Mol Struct (THEOCHEM) 807(1–3):109–119
12. Marcon V, Van der Vegt N, Wegner G, Raos G (2006) Modeling of molecular packing and conformation in oligofluorenes. J Phys Chem B 110(11):5253–5261
13. Meeto W, Suramitr S, Vannarat S, Hannongbua S (2008) Structural and electronic properties of poly(fluorine-vinylene) copolymer and its derivatives: Time-dependent density functional theory investigation. Chem Phys 349(1–3):1–8
14. Jespersen KG, Beenken WJD, Zaushitsyn Y, Yartsev A, Andersson M, Pullerits T, Sundström V (2004) The electronic states

of polyfluorene copolymers with alternating donor–acceptor units. J Chem Phys 121:12613–12617
15. Ahlrichs R, Bär M, Häser M, Horn H, Kölmel C (1989) Electronic structure calculations on workstation computers: the program system turbomole. Chem Phys Lett 162(3):165–169
16. von Arnim M, Ahlrichs R (1999) Geometry optimization in generalized natural internal coordinates. J Chem Phys 111(20): 9183–9190
17. Dirac PAM (1929) Quantum mechanics of many-electron systems. Proc R Soc Lond A 123:714–733
18. Slater JC (1951) A simplification of the Hartree–Fock method. Phys Rev 81:385–390
19. Vosko SH, Wilk L, Nusair M (1980) Accurate spin-dependent electron liquid correlation energies for local spin density calculations: a critical analysis. Can J Phys 58(8):1200–1211
20. Becke AD (1988) Density-functional exchange-energy approximation with correct asymptotic behavior. Phys Rev A 38(6): 3098–3100
21. Kohn W, Becke AD, Parr RG (1996) Density functional theory of electronic structure. J Chem 100(31):12974–12980
22. Treutler O, Ahlrichs R (1995) Efficient molecular numerical integration schemes. J Chem Phys 102(1):346–354
23. Bauernschmitt R, Ahlrichs R (1996) Treatment of electronic excitations within the adiabatic approximation of time dependent density functional theory. Chem Phys Lett 256(4–5):454–464
24. Klamt A, Schüürmann G (1993) COSMO: a new approach to dielectric screening in solvents with explicit expressions for the screening energy and its gradient. J Chem Soc Perkin Trans 2:799–805
25. Jacquemin D, Perpete EA, Chermette H, Ciofini I, Adamo C (2007) Comparison of theoretical approaches for computing the bond length alternation of polymethineimine. Chem Phys 332(1): 79–85
26. Liu Q, Liu W, Yao B, Tian H, Xie Z, Geng Y, Wang F (2007) Synthesis and chain-length dependent properties of monodisperse oligo(9, 9-di-n-octylfluorene-2,7-vinylene)s. Macromolecules 40(6):1851–1857
27. Yang L, Ren AM, Feng JK, Wang JF (2005) Theoretical investigation of optical and electronic property modulations of pi-conjugated polymers based on the electron-rich 3, 6-dimethoxy-fluorene unit. J Org Chem 70(8):3009–3020
28. Wang JF, Feng JK, Ren AM, Liu XD, Ma YG, Lu P, Zhang HX (2004) Theoretical studies of the absorption and emission properties of the fluorene-based conjugated polymers. Macromolecules 37(9):3451–3458
29. Chidthong R, Hannongbua S, Aquino A, Wolschann P, Lischka H (2007) Excited state properties, fluorescence energies, and lifetime of a poly(fluorene-pyridine) copolymer, based on TD-DFT investigation. J Comput Chem 28(10):1735–1742
30. Cornil J, Gueli I, Dkhissi A, Sancho-Garcia JC, Hennebicq E, Calbert JP, Lemaur V, Beljonne D (2003) Electronic and optical properties of polyfluorene and fluorene-based copolymers: a quantum-chemical characterization. J Chem Phys 118:6615–6623
31. Gierschner J, Cornil J, Egelhaaf HJ (2007) Optical bandgaps of π-conjugated organic materials at the polymer limit: experiment and theory. Adv Mater 19:173–191
32. Sancho-García JC (2006) Assessing a new nonempirical density functional: difficulties in treating π-conjugation effects. J Chem Phys 124:124112/1–124112/10
33. Sancho-García JC (2007) Treatment of singlet–triplet splitting of a set of phenylene ethylenes organic molecules by TD-DFT. Chem Phys Lett 439:236–242
34. Jansson E, Chandra Jha P, Ågren H (2007) Chain length dependence of singlet and triplet excited states of oligofluorenes: a density functional study. Chem Phys 336(2–3):91–98
35. Meier H, Stalmach U, Kolshorn H (1997) Effective conjugation length and UV/vis spectra of oligomers. Acta Polymer 48:379–384
36. Oelkrug D, Tompert A, Egelhaaf HJ, Hanack M, Steinhuber E, Hohloch M, Meier H, Stalmach U (1996) Towards highly luminescent phenylene vinylene films. Synth Met 83(3):231–237
37. Peach GMJ, Tellgren EI, Saek P, Helgaker T, Tozer DJ (2007) Structural and electronic properties of polyacetylene and polyyne from hybrid and coulomb-attenuated density functionals. J Phys Chem A 111(46):11930–11935
38. Luke V, Aquino A, Lischka H, Kauffmann HF (2007) Dependence of optical properties of oligo-*para*-phenylenes on torsional modes and chain length. J Phys Chem B 111(28):7954–7962
39. Beenken WJD, Lischka H (2005) Spectral broadening and diffusion by torsional motion in biphenyl. J Chem Phys 123: 144311–144319
40. Tirapattur S, Belletete M, Drolet N, Leclerc M, Durocher G (2003) Steady-state and time-resolved studies of 2,7-carbazole-based conjugated polymers in solution and as thin films: determination of their solid state fluorescence quantum efficiencies. Chem Phys Lett 370(5–6):799–804
41. Jenekhe SA, Lu L, Alam MM (2001) New conjugated polymers with donor–acceptor architectures: Synthesis and photophysics of carbazole-quinoline and phenothiazine-quinoline copolymers and oligomers exhibiting large intramolecular charge transfer. Macromolecules 34(21):7315–7324
42. Schenning APH, Tsipis AC, Meskers SCJ, Beljonne D, Meijer EW, Brdas JL (2002) Electronic structure and optical properties of mixed phenylene vinylene/phenylene ethynylene conjugated oligomers. Chem Mater 14(3):1362–1368
43. Pålsson LO, Wang C, Russell DL, Monkman AP, Bryce MR, Rumbles G, Samuel DW (2002) Photophysics of a fluorene copolymer in solution and films. Chem Phys 279(2–3):229–237
44. Sun RG, Wang YZ, Wang DK, Zheng QB, Kyllo EM, Gustafson TL, Wang F, Epstein AJ (2000) High PL quantum efficiency of poly(phenylene vinylene) systems through exciton confinement. Synth Met 111–112:595–602

Journal of Molecular Structure: THEOCHEM 939 (2010) 75–81

Contents lists available at ScienceDirect

Journal of Molecular Structure: THEOCHEM

journal homepage: www.elsevier.com/locate/theochem

Effects of the CN and NH_2 substitutions on the geometrical and optical properties of model vinylfluorenes, based on DFT calculations

Wichanee Meeto [a], Songwut Suramitr [a], Vladimír Lukeš [b], Peter Wolschann [c], Supa Hannongbua [a,*]

[a] Department of Chemistry, Faculty of Science, and Center of Nanotechnology, Kasetsart University, Bangkok 10900, Thailand
[b] Department of Chemical Physics, Slovak University of Technology, Radlinského 9, SK-81 237 Bratislava, Slovakia
[c] Institute for Theoretical Chemistry, University of Vienna, Währingerstrasse 17, A-1090 Wien, Austria

ARTICLE INFO

Article history:
Received 16 July 2009
Received in revised form 21 September 2009
Accepted 21 September 2009
Available online 6 October 2009

Keywords:
Bifluorenevinylene
Density functional theory
Torsional potential
Vertical excitation energy
Conducting polymer
Substitutional effect

ABSTRACT

A systematic study on the structural and photo-physical properties of model bifluorenevinylene compounds based on the density functional theory (DFT) and its time-dependent (TD-DFT) version is presented. The main aim of this work is to investigate the influence of substitution on bifluorenevinylene using strong electron acceptor CN or electron donor NH_2 groups on: (a) the optimal geometry, (b) torsional potentials and (c) photo-physical properties. Our results indicate that the substitution on the vinylene bridge, leads to the twisting of molecular fragment on the side of added group and are in good overall agreement with experiment. In the case of the amino mono-substituted bifluorenevinylene, the amino group leads to non-planarity at the non-substituted portion of the molecule. The chemical modification also have a pronounced impact on the electronic properties. The shape of the potential energy curves evaluated for the lowest vertically excited states is heavily dependent on the molecular conformation. Finally, we discuss how the structural and electronic information presented here can be useful in designing of novel optical materials as well as understanding of excitation–relaxation phenomena which may occur in various time-dependent optical experiments.

1. Introduction

Polyfluorenes, with their excellent photoluminescence quantum characteristics, excellent solubility in common organic solvents, can be used as blue-shift emitters [1,2]. Additionally, their thermal and chemical stability can be modified and improved by adding of different alkyl substiuents at the 9-th position of the fluorene ring [3]. However, the polyfluorenes systems containing simple connected fluorene units tend to aggregate in the condensed phase and provide less effective performance. Fortunately, these problems can be limited with the modification of their molecular structure, such as the polyfluorene-2,7-vinylenes (PFVs) [4]. Moreover, the various electron-donating or electron-accepting groups can be added to the vinylene bridge located within the aromatic molecular chain which subtly alters the intermolecular steric interactions which can be used to effectively tune the optical spectra from blue to the infrared region without the necessity to perturb the planarity of aromatic units [5,6].

Theoretical quantum studies of π-conjugated oligomers or polymers can provide a fundamental understanding of the physical process occurring, and make a considerable contribution to the design of novel optoelectronic materials. These include theoretical studies done using semiempirical, *ab initio* and density functional theory (DFT) methods, focusing on the electronic properties based on the ground-state equilibrium geometries [7–10]. Among them, the DFT approach and its time-dependent (TD) extension [11] for the excited states have been successfully demonstrated in investigations of optical and electronic properties of moderate to large organic conjugated oligomers [12]. These results are often used in cooperation with the experimental data to characterize the structural, electronic and optical properties of conjugated polymers and represent primary information to aid in our understanding of phenomena connected with conformation relaxation processes occurring during the electronic excitation and/or de-excitation [13]. Bifluorenevinylene derivatives are the focus of this research investigation, being shortest computationally efficient representation of oligo- and poly-vinylfluorenes which are of significant scientific interest.

The main aim of this work is the investigation of the direct influence of substitution using strong electron acceptor CN or electron donor NH_2 groups on the optimal geometry, torsional potentials and photo-physical properties. We do this by modifying the electronic structure of these model systems by the symmetric or asymmetric addition of the representative electron-accepting cyano and electron-donating amino groups on vinyl positions (see Fig. 1). We focus on the *all-trans* conformations and the electronic ground-state torsional potential curves in this investigation. The

* Corresponding author. Tel.: +66 2 5625555x2140; fax: +66 2 5793955.
E-mail address: fscisph@ku.ac.th (S. Hannongbua).

0166-1280/$ - see front matter © 2009 Elsevier B.V. All rights reserved.
doi:10.1016/j.theochem.2009.09.043

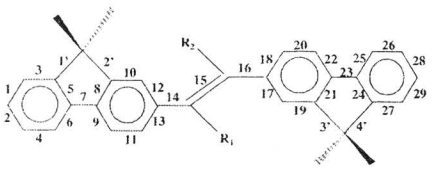

Molecule	R_1	R_2
F_2V	H	H
F_2V-$(CN)_2$	CN	CN
F_2V-$(NH_2)_2$	NH_2	NH_2
F_2V-CN	CN	H
F_2V-NH_2	NH_2	H
F_2V-CN-NH_2	CN	NH_2

Fig. 1. Schematic structure, bond and dihedral angle numbering of studied systems in *all-trans* conformation.

corresponding vertical excitation characteristics of these molecules are calculated using (TD-)DFT method. Finally, the physical origin of the lowest electronic transitions will be explained using molecular orbital analysis.

2. Methodology

The geometries and torsion potential of studied dimers F_2V, F_2V-$(CN)_2$, F_2V-$(NH_2)_2$, F_2V-CN, F_2V-NH_2 and F_2V-CN-NH_2 (formula and abbreviations are given in Fig. 1) are optimized by the DFT method using the Becke three parameter hybrid (B3LYP) [14] functional in conjunction with the 6-31G(d) basis set [15]. The torsion potentials were calculated for the fixed angles from the

Table 1
The B3LYP/6-31G(d) optimal dihedral angles (in deg) and BLA parameters (in Å) for *all-trans* conformations.

Molecule	Θ_1	Θ_2	BLA
F_2V	0	0	0.224
F_2V-$(CN)_2$	38	−38	0.218
F_2V-$(NH_2)_2$	45	−45	0.236
F_2V-CN	28	−7	0.212
F_2V-NH_2	36	−31	0.227
F_2V-CN-NH_2	52	−44	0.223

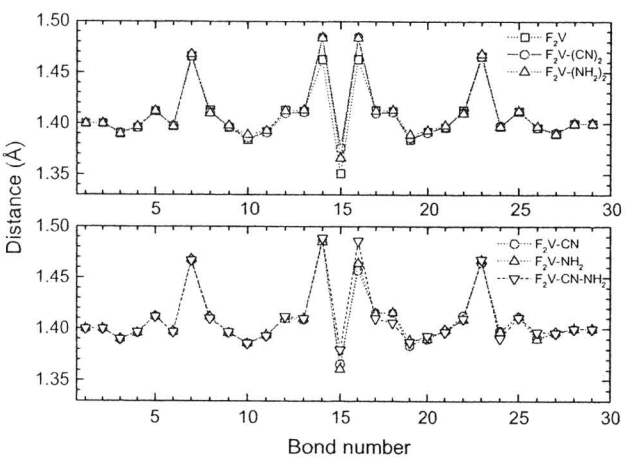

Fig. 2. Computed B3LYP/6-31G(d) bond lengths of the molecules under study in *all-trans* conformation. For notation see Fig. 1.

Table 2
The lowest excitation energies in eV and oscillator strengths (values in parentheses) for the optimal *all-trans* geometries. The values written in italics stand for the excitation contributions in percentage involved in each calculated transition (H denotes HOMO and L is LUMO).

Molecule	S_1	S_2	S_3	S_4	S_5	S_6	S_7
F_2V	3.23 (1.870)	3.98 (0.000)	4.18 (0.000)	4.19 (0.006)	4.41 (0.00)	4.44 (0.019)	4.44 (0.000)
	99%: H → L	*60%*: H−1 → L	*50%*: H → L+3	*68%*: H → L+2	*43%*: H → L+2	*33%*: H−2 → L	*60%*: H−3 → L
		38%: H → L+1					
F_2V-$(CN)_2$	2.82 (0.907)	3.22 (0.000)	3.64 (0.009)	3.67 (0.000)	3.67 (0.000)	3.88 (0.000)	4.29 (0.336)
	99%: H → L	*97%*: H−1 → L	*70%*: H−2 → L	*75%*: H−3 → L	*68%*: H−4 → L	*73%*: H−5 → L	*72%*: H−6 → L
F_2V-$(NH2)_2$	2.90 (0.586)	3.30 (0.000)	3.53 (0.009)	3.61 (0.000)	4.21 (0.016)	4.24 (0.000)	4.41 (0.713)
	99%: H → L	*97%*: H → L+1	*94%*: H → L+2	*92%*: H → L+3	*91%*: H → L+4	*90%*: H → L+5	*93%*: H−2 → L+1
F_2V-CN	3.08 (1.424)	3.72 (0.096)	4.08 (0.002)	4.08 (0.016)	4.22 (0.007)	4.26 (0.006)	4.39 (0.063)
	99%: H → L	*91%*: H−1 → L	*98%*: H−2 → L	*62%*: H−3 → L	*42%*: H−5 → L	*44%*: H−4 → L	*75%*: H → L+1
F_2V-NH_2	3.29 (1.099)	3.86 (0.251)	4.03 (0.013)	4.08 (0.021)	4.40 (0.079)	4.54 (0.023)	4.58 (0.027)
	99%: H → L	*87%*: H → L+1	*67%*: H → L+2	*69%*: H → L+3	*83%*: H−1 → L	*39%*: H → L+6	*41%*: H → L+5
F_2V-CN-NH_2	3.53 (0.824)	4.01 (0.165)	4.25 (0.006)	4.29 (0.085)	4.38 (0.010)	4.41 (0.131)	4.63 (0.015)
	98%: H → L	*73%*: H → L+1	*70%*: H−1 → L	*67%*: H → L+1	*61%*: H → L+3	*70%*: H−2 → L	*70%*: H−4 → L

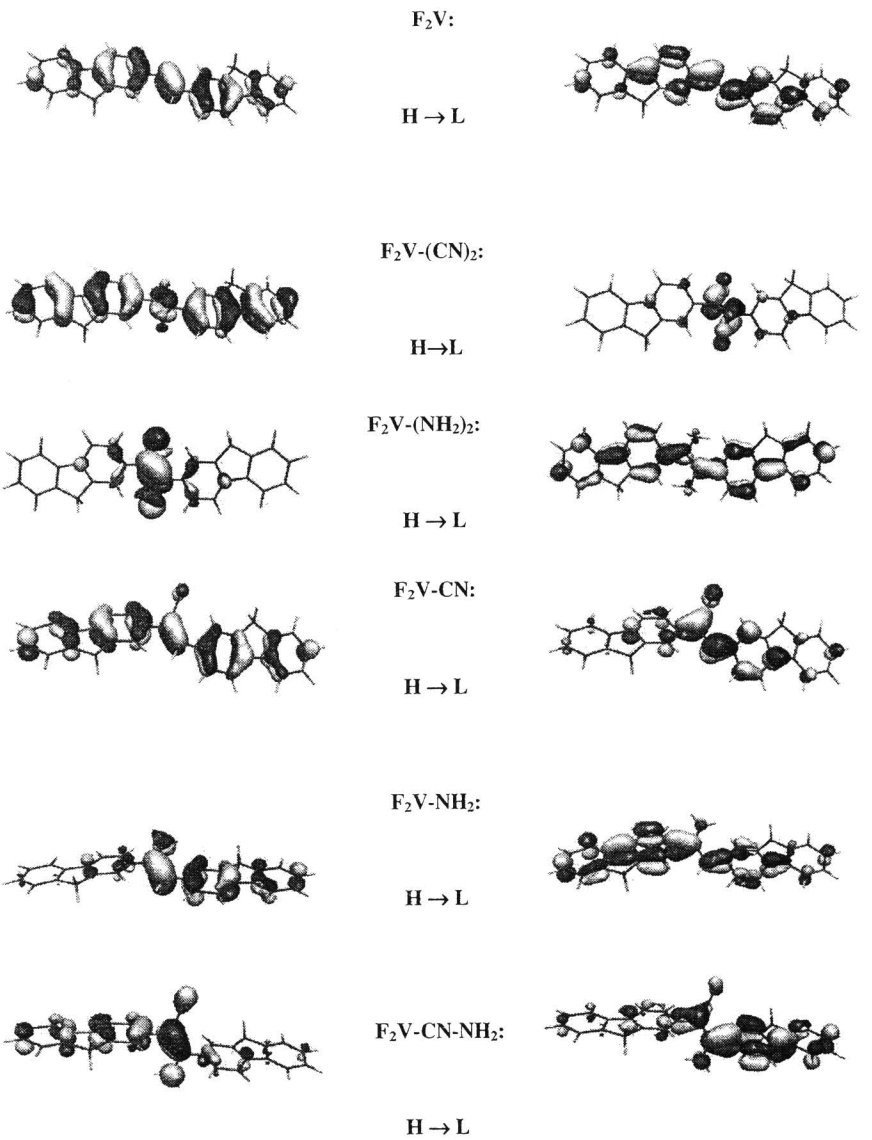

Fig. 3. Plots of the B3LYP/6-31G(d) molecular orbitals contributing significantly to the lowest energy transitions of studied molecules in *all-trans* conformation. H denotes HOMO and L is LUMO.

interval 0° to 180° using a 10° step size. In the case of asymmetric molecules, dihedral angles for both sides were investigated due to the different steric effects. Singlet vertical excitation energies are calculated from the optimized geometries using the TD-B3LYP method. All calculations are performed using the Gaussian 03 program package [16]. Due to the computational cost reduction, the alkyl groups at 9-th position on fluorene ring were replaced by hydrogen atoms. This is because reports suggest that substituents at the 9-th position play an important role in the thermal stability and solubility but do not affect the electronic structure and optical property of fluorene-based polymer [17,18]. All minima were confirmed as such though normal mode analysis, displaying no imaginary vibration frequencies.

3. Results and discussion

Comparison of the optimized ground-state 1^1A geometries in terms of bond lengths and torsional angles can help us to understand the structural and energetic differences observed between the different systems. Schematic visualization of the molecular structure of the bifluorenevinylene skeleton studied here are given in Fig. 1. The data presented in Table 1 show the energy profile for the dihedral angles Θ_1 (between the bond nos. 12, 14 and 15) and Θ_2 (between the bond nos. 15, 16 and 17) between fluorene unit and the vinylene bridge on the substitution. The B3LYP/6-31G(d) calculation indicates the structure of F_2V molecule is completely planer. Substitution at the vinylene bridge leads to the perturbation of planarity due to the steric hindrance and the effect of electronegativity from nitrogen atoms in the vicinity of the newly added substituents. In the case of mono-substituted molecules, the presence of CN substituents increases the angle Θ_1 to the value of 30° while the torsion for NH_2 group is higher, 35°. Interestingly, the second angle Θ_2 is evidently non-planar only for molecule F_2V–NH_2. The symmetric bi-substitution is responsible for a torsion angle increase of ~10° with respect to the mono-substituted systems. The most distorted structure is obtained for the asymmetric F_2V–CN–NH_2 molecule, where the torsion on the side of cyano group results in a dihedral angle of 52°.

The computed bond lengths for the molecules studied here are presented in Fig. 2. In all cases the smallest C–C bond distances are located in the central part of the fluorene rings (see bond nos. 3, 10, 19 and 27) and double bond on vinylene bridge (see bond no. 15). The largest bond lengths are found for the inter-ring distances (bond nos. 7 and 23) which have a larger single bond character than the next bonds in the fluorene unit. The single bond nos. 14 and 16 on vinylene bridge exhibit also the largest distances. The substitution of vinylene bridge affects only the bonds in the vicinity of added group, especially the bonds of vinylene bridge. The double bond no. 15 as well as the neighbouring single bond nos. 14 and 16 are elongated while the bonds on rigid fluorene rings are very slightly shortened. Our calculations indicate that the differences in bond length changes for CN and NH_2 substitutions are significant only for bond no. 15. The CN substitution elongates it at 0.03 Å while the amino group changes it only 0.02 Å with respect to the F_2V molecule. Similar changes in bond lengths are observed for the mono-substituted NH_2 and CN compounds. However, in this case the bonds on the side of the substituted part are affected. The asymmetric substitution of F_2V–CN–NH_2 molecule leads to the formation of electronic system where NH2 acts an electron donor to the aromatic system and the fluorene atoms as electron acceptor. In comparison with previously discussed molecules the bonds on the side of CN group and located on fluorene rings (bond nos. 17, 18, 24 and 26) are more influenced than in the F_2V–CN and F_2V–$(CN)_2$ molecules.

Bond length changes in aromatic systems can be efficiently described using the bond length alternation (BLA) definition [19]. The BLA values for a given molecular fragment is defined as the difference in length between single and double bonds between non-hydrogen atoms. The positive sign of BLA for example indicates that the molecular unit has an aromatic character. The BLA value for central vinylene bridge may be evaluated using equation 1,

$$\mathrm{BLA} = (d_{14} + d_{16}) - 2d_{15}$$

where d symbols denote the bond lengths determined in Fig. 1.

Brédas et al. [20] studied the relationship between band gap and bond length alternation of conjugated polymers and their results indicate that in aromatic-based conjugated polymers, the energy gap decreases as a function of increasing quinoid character of polymer backbone. As can be seen from data in Table 1, the mono-substitution with electron-withdrawing CN group leads to decrease of the BLA value by 0.006 Å with respect to the F_2V molecule. The next presence of CN group has an additive influence on the BLA decrease. The presence of CN groups leads to increasing quinoid character. Consequently, the lowest excitation energies of F_2V–CN and F_2V–$(CN)_2$ are decreased when compared to the original compound. On the other hand, a small increase of BLA value is obtained for amino derivatives F_2V–NH_2 and F_2V–$(NH_2)_2$. For the push–pull system of F_2V–CN–NH_2, the resulting influence of both groups has a compensatory effect since the BLA value is similar to the non-substituted F_2V molecule.

The structural changes in the central part of the molecule, induced by the strong electron-withdrawing cyano or donating amino groups, are also reflected in the vertically excited electronic states, reflecting the balance between the perturbation of conjugation due to the distortion of the planer scaffold and the electronic effects of the substituents. The first seven vertical excitation energies with non-negligible oscillator strengths are summarized in Table 2. The lowest excitation energy for non-substituted molecule F_2V is 3.23 eV, compared to 3.08 eV [21] for tetrahydrofuran, suggesting the model systems employed and the level of theory employed is sufficiently accurate to gain useful insights.

The mono- or symmetric bi-substitutions lead to a bathochromic energy shift. Only in the case of F_2V–NH_2 molecule, the lowest excitation is blue-shifted by 0.06 eV. The global hypsochromic shift of excitation energies is indicated for the F_2V–CN–NH_2 system. The lowest excitation energy is higher about 0.20 eV with respect to the F_2V. It seems that the torsion of molecular chains has more dominant influence of the photo-physical properties than the global push–pull effects of used substituents. Finally, in all cases, the substitution of vinylene bridge leads to a decrease in the oscillator strength for the lowest singlet excitation transition (S_1) and to the increase of the oscillator strengths for the next optical transitions.

In order to understand the physical origin of optical transitions for the selected excitation energies, it is useful to examine the (highest) occupied (HOMO) and lowest unoccupied molecular orbitals (LUMO). As reported in Table 2, the lowest energy electronic excitation is from the HOMO to the LUMO for all molecules and displays $\pi\pi^*$ character. However, the electronic distribution observed for the next transitions, as different as given by the molecular orbitals, are very different for the different substitutions. As presented in Fig. 3, the HOMO orbital of F_2V molecule is located mostly on the double bond of vinylene bridge (bond no. 15) and neighbouring bonds on fluorene units perpendicular oriented with respect to the chain (see bond nos. 12, 13, and 17, 18). The LUMO orbital is spread over the single bonds of vinylene bridge (bond nos. 14 and 16) and bonds on the fluorene units which are parallel with the molecular chain (see bond nos. 10, 11 and 19, 20). The presence of electron-withdrawing cyano group in F_2V–CN and F_2V–$(CN)_2$ molecules increases the electron delocalization in HOMO over the fluorene units. On the other hand, the electron-donating amino groups in F_2V–NH_2

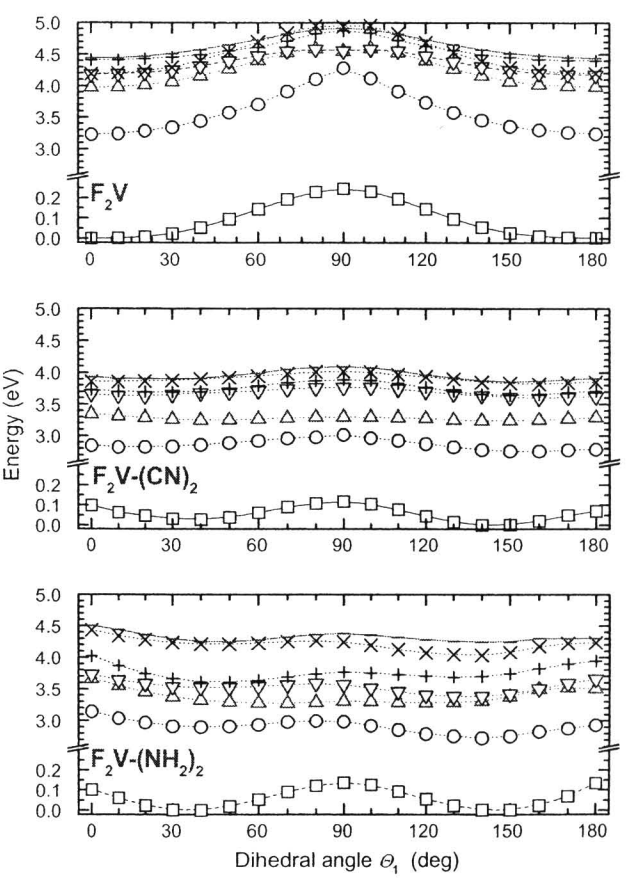

Fig. 4. One-dimensional dependence of the electronic ground-state and vertically excited energies of studied symmetric systems on the torsion calculated at the B3LYP/6-31G(d) theoretical level. The ground-state energy minimum is taken as energy reference (see also Table 3). The open square denote electronic ground-state and the next symbols indicate the first six excited states (S_1, ○; S_2, △; S_3, ▽; S_4, +; S_5, ×; S_6, –).

and F_2V–$(NH_2)_2$ molecules is responsible for the electron delocalization over the vinylene bond no. 15.

The opposite situation is observed in the LUMOs for both types of derivatives. With respect to this fact, we can deduce that the optical transition for cyano derivatives is oriented from the fluorene units to the CN chromophore while for the amino derivatives it is spread from the central part to the fluorene units. This character is also reflected for the higher vertical excitations. The transitions from lower occupied orbitals to the LUMO orbital play important role for the CN derivatives. The transitions from HOMO to the next unoccupied orbitals occur for the amino derivatives. In the case of the F_2V–CN–NH_2 molecule, the presence of the strong push–pull systems leads to the combined effect with strongly determined direction of optical transition. This electron transition starts from the fluorene unit and neighbouring NH_2 group and goes to the CN group and opposite fluorene unit.

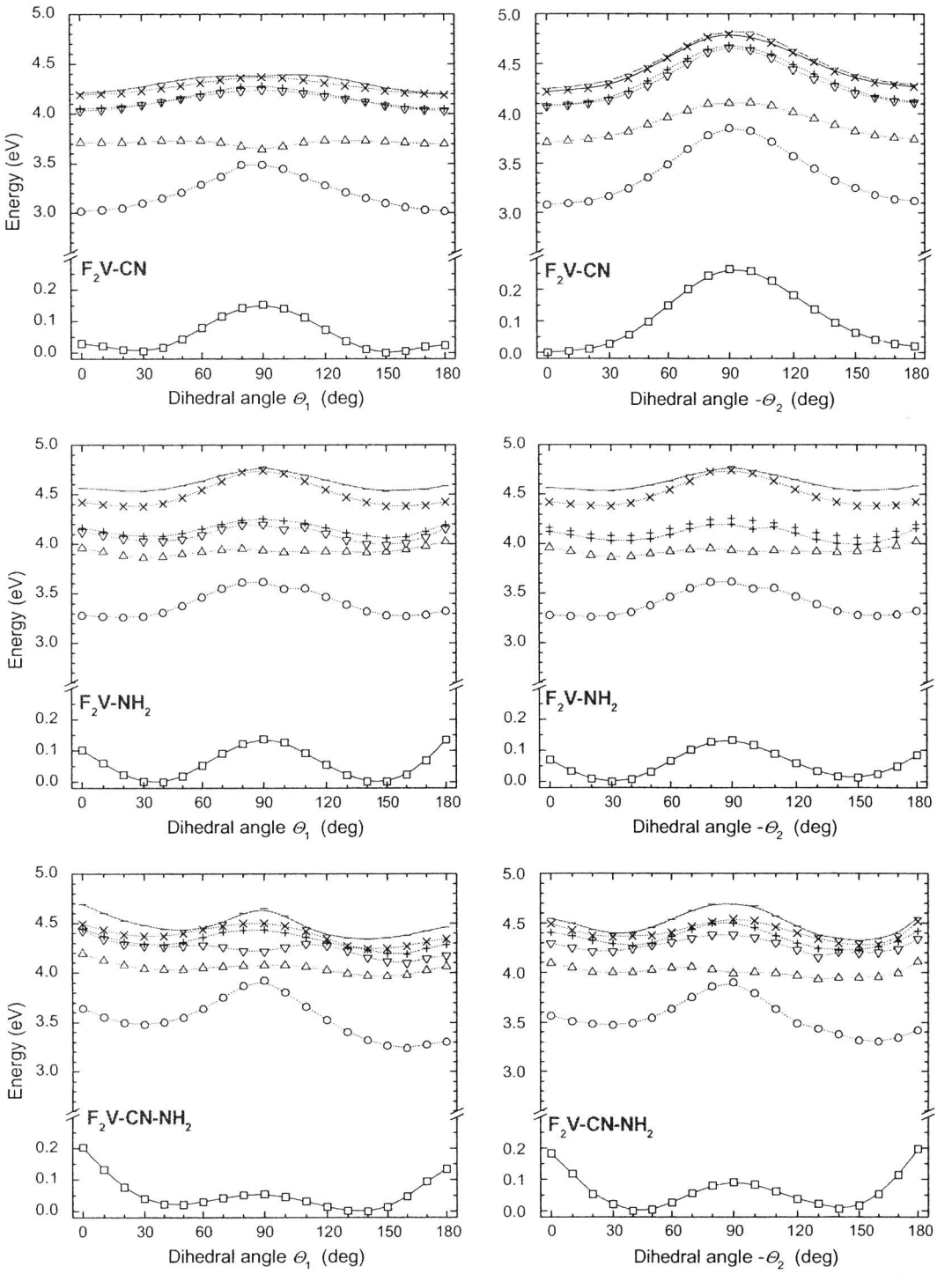

Fig. 5. One-dimensional dependence of the electronic ground-state and vertically excited energies of studied asymmetric systems on the torsion calculated at the B3LYP/6-31G(d) theoretical level. The ground-state energy minimum is taken as energy reference (see also Table 3). The open square denote electronic ground-state and the next symbols indicate the first six excited states (S_1, ○; S_2, △; S_3, ▽; S_4, +; S_5, ×; S_6, -).

The electronic ground-state torsional potentials of the fluorene unit around the common single bond were also investigated using the B3LYP/6-31G(d) method with the results being depicted in Figs. 4 and 5 and the geometrical and energetic values in Table 3. As can be seen in Fig. 4, the non-substituted molecule F_2V has two planar minima and the barrier for perpendicular arrangement (ΔE = 0.245 eV or 5.65 kcal mol^{-1}). We note that the similar shape of potential and barrier location with ΔE = 0.22 eV (5.0 kcal mol^{-1}) were obtained for the torsion of phenylene ring around the vinylene single bond at the B3LYP/cc-pVDZ theoretical level [22]. The presence of cyano or amino groups on the vinylene bridge leads to structures that are more stable to a non-planer conformation. The obtained potential curves exhibit two non-planar minima corresponding to the most stable *trans* or *cis* conformations and two first-order saddle points. The most stable conformation of F_2V–$(NH_2)_2$ molecule is at 45° while the F_2V–$(CN)_2$ molecule prefers *trans* conformation (144°). The mutual comparison of the energy barriers with respect to the F_2V molecule shows that the vinylene bridge substitution decreases the barrier at perpendicular arrangement. The cyano substitution decreases the barrier relative to F_2V by 0.092 eV (for F_2V–CN) and by 0.128 eV (for F_2V–$(CN)_2$). Although the amino substitution leads to the higher decrease of the perpendicular barrier relative to F_2V (0.108 eV for F_2V–NH_2 and 0.169 eV for F_2V–$(NH_2)_2$), the torsion at the planar arrangements is more restricted. The electronic ground-state potential curves for mono-substituted molecules around the second dihedral angle Θ_2 have different shape. For the F_2V–CN molecule, the shape is similar to the potential curve of non-substituted F_2V molecule. A different situation occurs for the F_2V–NH_2 molecule in that the second evaluated curve copies the shape of the dependence around the first dihedral angle. It seems that the strong electron donor amino group is able directly to affect through the double bond no. 15 the torsional motion on the opposite molecular side. The modification of the torsional potential with the amino or cyano groups is also observed for mixed F_2V–CN–NH_2 molecule. As can be seen in Fig. 5, the torsional potential profile for the Θ_1 and Θ_2 dihedral angles are two-times lower in energy for the perpendicular arrangement compared to the planar arrangement. In addition, the potential curve for the torsion around the angle Θ_1 (at the side of CN substitution) exhibits more stable conformation at 132°. The energy difference with respect to the second minimum at 52° is 0.021 eV. This is a different situation to that presented for F_2V–CN and F_2V–NH_2. It appeals that these features have a different impact on the excitation–relaxation phenomena which occur in various time-dependent optical experiments.

Table 3
Relative energies ΔE and dihedral angles Θ_1 and Θ_2 of external points for torsional dependencies with respect to the most stable structure. The angles are in degrees and energies in eV or kcal mol^{-1} (values in parentheses). See also Figs. 4 and 5.

Molecule	Θ_1	Θ_2	ΔE
F_2V	0	0	0.000 (0.00)
	90	0	0.245 (5.65)
	180	0	0.003 (0.07)
F_2V–$(CN)_2$	0	−46	0.099 (2.28)
	38	−38	0.000 (0.00)
	90	−29	0.117 (2.70)
	144	−37	0.001 (0.02)
	180	−45	0.069 (1.59)
F_2V–$(NH_2)_2$	0	−57	0.224 (5.17)
	45	−45	0.000 (0.00)
	90	−39	0.076 (1.75)
	128	−37	0.038 (0.88)
	180	−45	0.298 (6.88)
F_2V–CN	0	0	0.029 (0.67)
	28	−7	0.001 (0.02)
	90	0	0.153 (3.53)
	148	−7	0.000 (0.00)
	180	−1	0.024 (0.55)
	25	−90	0.293 (6.76)
	29	−180	0.049 (1.13)
F_2V–NH_2	0	−31	0.102 (2.35)
	36	−31	0.000 (0.00)
	90	−28	0.137 (3.16)
	146	−24	0.002 (0.05)
	180	−38	0.134 (3.09)
	36	0	0.070 (1.61)
	35	−90	0.132 (3.04)
	35	−148	0.013 (0.30)
	39	−180	0.085 (1.96)
F_2V–CN–NH_2	0	−31	0.205 (4.73)
	52	−44	0.021 (0.50)
	90	−28	0.056 (1.29)
	132	−43	0.000 (0.00)
	180	−38	0.124 (2.65)
	57	0	0.184 (4.24)
	42	−90	0.091 (2.10)
	43	−133	0.024 (0.57)
	58	−180	0.198 (4.57)

The excited-state potential energy curves calculated at the TD-B3LYP/6-31G(d) level based on ground-state optimized geometries are also shown in Figs. 4 and 5. The curve for the lowest excited state of S_1 with dominant oscillator strengths for F_2V exhibits the energy minimum for a planar geometry and a maximum for the perpendicular one. The energy difference between these points is ca 1.06 eV. In the case of F_2V–CN and F_2V–NH_2, the S_1 state practically reflects the curve for the F_2V molecule, but the energy differences between the perpendicular and planar arrangements are approximately two-times lower. The symmetric bi-substitution decreases very effective the sensitivity of the evaluated potential curves on the torsion. Moreover, in all investigated molecules, the lowest S_1 state does not cross the next higher states. The potential energy curves for the next higher excited states of F_2V molecule are quite closely spaced to each other and show multiple intersections (around 70–120°). On the other hand, the substitution can cause the small separation of crossing region of potential curves between the next lowest excited states.

4. Conclusions

The (TD)-B3LYP method has been used for the systematic theoretical investigation of the photo-physical properties of substituted model bifluorenevinylene compounds. The substitutions of the vinylene unit by strong electron-acceptoring CN and/or electron-donating NH_2 groups were considered. Our calculations indicate that the non-substituted F_2V compound is planar and that substitution leads to the twisting of the molecular fragment on the side of substitution. In the case of the F_2V–NH_2 molecule, the amino group is also responsible for the non-planarity on the non-substitute side. Additionally, the chemical modification of vinylene bridge affects the electronic ground-state torsional potentials of the fluorene unit around the single bond. The non-substituted molecule F_2V has two planar minima and the barrier for perpendicular arrangement. The presence of cyano or amino groups on vinylene bridge is responsible for the restriction of the torsional motion at the barriers located for planar and perpendicular arrangements. The energy barrier highs are also dependent on the substitution.

The TD-DFT torsional potential energy curves in the vertically excited states were also investigated in this work. From our calculations, we do not find any indication of state crossings of the S_1 state with higher ones for all investigated systems. The symmetric bi-substitution markedly decreases the potential curves on the torsion. The potential energy curves for the next higher excited states of F_2V molecule are quite closely spaced to each other and show multiple intersections (around 70–120°). On the other hand, the substitution can modulate the separation of crossing region of

potential curves between the next lowest excited states. The absence of the intersections of excited states around the stable structures and relative well separation of the lowest excited state around the minima enable us to perform the molecular dynamics studies of investigated molecules based on an adiabatic approach. These results show that theoretical studies can help us to understand the relationship between the torsional broadening of absorption spectra, chemical structure and time-dependent optical phenomena, having implications for the design and synthesis of novel optical materials.

Acknowledgements

The authors thank Prof. Harald Kauffmann for valuable comments and discussion. This work was supported by the Thailand Research Fund (RTA5080005 to S.H. and MRG5180287 to S.S.). W.M. is grateful to Thai Graduate Institute of Science and Technology (TGIST), the Austrian Science Fund within the framework of the Special Research Program F16, Advanced Light Sources (ADLIS), and Bilateral Research Cooperation (BRC) from Faculty of Science, Kasetsart University for scholarships and supporting. The National Center of Excellence in Petroleum, Petrochemical Technology and Advanced Materials is gratefully acknowledged for research supporting and facilities. The calculations were performed in part on the Schrödinger III cluster of the University of Vienna. Thanks are also due to Dr. Matthew Paul Gleeson for helpful comments and reading of the manuscript.

References

[1] M. Ranger, D. Rondeau, M. Leclerc, Macromolecules 30 (1997) 7686.
[2] V.P. Barberis, J.A. Microyannidis, Synth. Met. 156 (2006) 1408.
[3] C. Chi, C. Im, V. Enkelmann, A. Ziegler, G. Lieser, G. Wegner, Chem. Eur. J. 11 (2005) 6833.
[4] S.H. Jin, H.J. Park, J.Y. Kim, K. Lee, S.P. Lee, D.K. Moon, H.J. Lee, Y.S. Gal, Macromolecules 35 (2002) 7532.
[5] Y. Jin, J.Y. Kim, S. Song, Y. Xia, J. Kim, H.Y. Woo, K. Lee, H. Suh, Polymer 49 (2008) 467.
[6] L. Zhang, Q. Zhang, H. Ren, H. Yan, J. Zhang, H. Zhang, J. Gu, Sol. Energy Mater. Sol. Cells 92 (2008) 581.
[7] V. Lukes, A. Aquino, H. Lischka, J. Phys. Chem. A 109 (2005) 10232.
[8] W. Meeto, S. Suramitr, S. Vannarat, S. Hannongbua, Chem. Phys. 349 (2008) 1.
[9] S. Suramitr, T. Kerdcharoen, T. Srikhirin, S. Hannongbua, Synth. Met. 155 (2005) 27.
[10] Y. Yang, J.K. Feng, Y. Liao, A.M. Ren, Polymer 46 (2005) 9955.
[11] F. Furche, R. Ahlrichs, J. Chem. Phys. 117 (2002) 7433.
[12] J. Gierschner, J. Cornil, H.J. Egelhaaf, Adv. Mater. 19 (2007) 173.
[13] S. Tretiak, A. Saxena, R.L. Martin, A.R. Bishop, Phys. Rev. Lett. 89 (2002) 97402.
[14] A.D. Becke, J. Chem. Phys. 98 (1993) 5648.
[15] P.M.W. Gill, B.G. Johnson, J.A. Pople, M.J. Frisch, Chem. Phys. Lett. 197 (1992) 499.
[16] M.J. Frisch, G.W. Trucks, H.B. Schlegel, G.E. Scuseria, M.A. Robb, J.R. Cheeseman, J.A. Montgomery Jr., T. Vreven, K.N. Kudin, J.C. Burant, J.M. Millam, S.S. Iyengar, J. Tomasi, V. Barone, B. Mennucci, M. Cossi, G. Scalmani, N. Rega, G.A. Petersson, H. Nakatsuji, M. Hada, M. Ehara, K. Toyota, R. Fukuda, J. Hasegawa, M. Ishida, T. Nakajima, Y. Honda, O. Kitao, H. Nakai, M. Klene, X. Li, J.E. Knox, H.P. Hratchian, J.B. Cross, V. Bakken, C. Adamo, J. Jaramillo, R. Gomperts, R.E. Stratmann, O. Yazyev, A.J. Austin, R. Cammi, C. Pomelli, J.W. Ochterski, P.Y. Ayala, K. Morokuma, G.A. Voth, P. Salvador, J.J. Dannenberg, V.G. Zakrzewski, S. Dapprich, A.D. Daniels, M.C. Strain, O. Farkas, D.K. Malick, A.D. Rabuck, K. Raghavachari, J.B. Foresman, J.V. Ortiz, Q. Cui, A.G. Baboul, S. Clifford, J. Cioslowski, B.B. Stefanov, G. Liu, A. Liashenko, P. Piskorz, I. Komaromi, R.L. Martin, D.J. Fox, T. Keith, M.A. Al-Laham, C.Y. Peng, A. Nanayakkara, M. Challacombe, P.M.W. Gill, B. Johnson, W. Chen, M.W. Wong, C. Gonzalez, J.A. Pople, 567 revision B.05. Gaussian, Inc., Pittsburgh, 2003.
[17] P. Poolmee, M. Ehara, S. Hannongbua, H. Nakatsuji, Polymer 46 (2005) 6474.
[18] K. Sriwichitkamol, S. Suramitr, P. Poolmee, S. Hannongbua, J. Theor. Comput. Chem. 5 (2006) 595.
[19] D. Jacquemin, E.A. Perpete, H. Chermette, I. Ciofini, C. Adamo, Chem. Phys. 332 (2007) 79.
[20] J.L. Brédas, J. Chem. Phys. 82 (1985) 3808.
[21] Q. Liu, W. Liu, B. Yao, H. Tian, Z. Xie, Y. Geng, F. Wang, Macromolecules 40 (2007) 1851.
[22] S.P. Kwasniewski, L. Claes, J.P. Francois, M.S. Deleuze, J. Chem. Phys. 118 (2003) 7823.

Absorption and emission spectra of ultraviolet B blocking methoxy substituted cinnamates investigated using the symmetry-adapted cluster configuration interaction method

Malinee Promkatkaew,[1,2] Songwut Suramitr,[1,2] Thitinun Monhaphol Karpkird,[1,3] Supawadee Namuangruk,[4] Masahiro Ehara,[5,a)] and Supa Hannongbua[1,2,a)]
[1]*Department of Chemistry, Faculty of Science, Kasetsart University, Bangkok 10900, Thailand*
[2]*Center of Nanotechnology, Kasetsart University, Bangkok 10900, Thailand*
[3]*Functional Compounds Special Research Unit (FCSRU), Kasetsart University, Bangkok 10900, Thailand*
[4]*National Nanotechnology Center (NANOTEC), National Science and Technology Development Agency (NSTDA), 130 Paholyothin Rd., Klong 1, Klongluang, Pathumthani 12120, Thailand*
[5]*Institute for Molecular Science, 38 Myodaiji, Okazaki 444-8585, Japan*

(Received 30 June 2009; accepted 27 October 2009; published online 8 December 2009)

The absorption and emission spectra of ultraviolet B (UVB) blocking cinnamate derivatives with five different substituted positions were investigated using the symmetry-adapted cluster configuration interaction (SAC-CI) method. This series included *cis*- and *trans*-isomers of *ortho*-, *meta*-, and *para*-monomethoxy substituted compounds and 2,4,5-(*ortho*-, *meta*-, *para*-) and 2,4,6-(*ortho*-, *para*-) trimethoxy substituted compounds. The ground and excited state geometries were obtained at the B3LYP/6-311G(d) and CIS/D95(d) levels of theory. All the compounds were stable as *cis*- and *trans*-isomers in the planar structure in both the S_0 and S_1 states, except the 2,4,6-trimethoxy substituted compound. The SAC-CI/D95(d) calculations reproduced the recently observed absorption and emission spectra satisfactorily. Three low-lying excited states were found to be relevant for the absorption in the UV blocking energy region. The calculated oscillator strengths of the *trans*-isomers were larger than the respective *cis*-isomers, which is in good agreement with the experimental data. In the *ortho*- and *meta*-monomethoxy compounds, the most intense peak was assigned as the transition from next highest occupied molecular orbital (next HOMO) to lowest unoccupied molecular orbital (LUMO), whereas in the *para*-monomethoxy compound, it was assigned to the HOMO to LUMO transition. This feature was interpreted as being from the variation of the molecular orbitals (MOs) due to the different substituted positions, and was used to explain the behavior of the excited states of the trimethoxy compounds. The emission from the local minimum in the planar structure was calculated for the *cis*- and *trans*-isomers of the five compounds. The relaxation paths which lead to the nonradiative decay were also investigated briefly. Our SAC-CI calculations provide reliable results and a useful insight into the optical properties of these molecules, and therefore, provide a useful tool for developing UVB blocking compounds with regard to the tuning of the photoabsorption. © *2009 American Institute of Physics*. [doi:10.1063/1.3264569]

I. INTRODUCTION

Cinnamates have received much attention, as they are the most widely used ultraviolet B (UVB) blocking compounds among the various cosmetic sunscreen agents. Recently, 2-ethylhexyl-*para*-methoxy cinnamate, as well as other cinnamate derivatives, has been developed as a commercial product.[1,2] Cinnamates achieve UVB blocking from a $\pi\pi^*$ absorption followed by a *cis-trans* isomerization at the propenyl double bond in the S_1 state and a relaxation to the ground state involving nonradiative decay.[3,4] As a UVB blocking compound, the optical properties, in particular, the photoabsorption efficiency in the UVB energy region (290–320 nm) is an important factor. In order to achieve the favorable optical properties, molecular design using the variation of the substituents has been extensively performed. The photochemistry of the process has also been studied, and the involvement of a intramolecular charge transfer (ICT) state resulting from a rotation at the C=C double bond is well recognized.[5,6]

Several experimental and theoretical studies have been conducted to elucidate the optical properties and photochemistry of cinnamates. Time-dependent density functional theory (TD-DFT) has been utilized to investigate the photochemistry of *trans*-ethyl-*para*-(dimethylamino) cinnamate by examining the twist coordinates, corroborating the experimental observation that the formation of an ICT state is feasible in the excited state.[5] Recently, the photophysical properties of methoxy substituted cinnamates, i.e., *ortho*-, *meta*-, and *para*-monomethoxy cinnamates and 2,4,5- and 2,4,6-trimethoxy 2-ethylhexyl-cinnamates, have been investigated experimentally to develop better UVB filter compounds.[7] The excited states and spectroscopic properties of *para*-

[a)]Authors to whom correspondence should be addressed. Electronic addresses: ehara@ims.ac.jp and fscisph@ku.ac.th.

hydroxy cinnamate were investigated using TD-DFT and complete active space self-consistent field (CASSCF) methods.[8] It was also observed that the UV absorption and fluorescence are affected by the solvent, with a shift to longer wavelengths in polar solvents.[9,10] These studies have provided some useful insights into the optical properties of these molecules. However, reliable theoretical work is still necessary to understand the details of the optical properties of these molecules, such as the difference in the absorption and emission of the *trans*- and *cis*-isomers and the effect of the solvent.

The symmetry-adapted cluster configuration interaction (SAC-CI) method was developed by Nakatsuji[11,12] to obtain a detailed interpretation and prediction of the molecular spectroscopy and photochemistry of the molecules. The SAC-CI method has been established as a reliable and useful method for investigating a wide variety of chemical phenomena through many successful applications.[13,14] The method has been utilized for the accurate theoretical spectroscopy of many π-conjugated systems[15–17] and has also been applied to the photochemistry of biological systems, such as porphyrins, photosynthetic reaction centers, retinal, and luciferin.[18–21] Recently, the photophysical properties and excited state dynamics of fluorescent molecules, such as fluorine-thiophene oligomers[22] and poly(*para*-phenylenevinylene) and poly(*para*-phenylene)[23] that are useful for organic light-emitting diodes were investigated and the absorption/emission spectra of these molecules were elucidated. These works confirm that the SAC-CI method is useful for investigating the electronic excitations and excited state dynamics of large π-conjugated systems.

In this work, the absorption and emission spectra of the *cis*- and *trans*-isomers of methoxy substituted cinnamates have been theoretically investigated using the SAC-CI method. The target molecules were *ortho*-(**1**), *meta*-(**2**), and *para*-(**3**) monomethoxy substituted cinnamates, and 2,4,5-(**4**) and 2,4,6-(**5**) trimethoxy cinnamates, as shown in Fig. 1, whose experimental spectra were reported recently.[7] The vertical absorption and emission spectra were calculated at the theoretically optimized molecular geometries. The difference in electronic transitions among these molecules and the effect of methoxy substitution at the *ortho*-, *meta*-, and *para*-positions were analyzed. The change in geometry in the first excited state was qualitatively interpreted using electrostatic force (ESF) theory.[24,25] The relaxation pathways that lead to the nonradiative decay were also briefly addressed.

II. COMPUTATIONAL DETAILS

The molecular structure of the *cis*- and *trans*-isomers of methoxy substituted 2-ethylhexyl-*ortho*-(**1**), *meta*-(**2**), and *para*-(**3**) monomethoxy cinnamates and 2,4,5-(**4**) and 2,4,6-(**5**) trimethoxy cinnamates is shown in Fig. 1(a). In this work, the photophysical properties of the model compounds shown in Fig. 1(b) were investigated to reduce the computational requirements without sacrificing the essence of the excitation, as the electronic structure relevant to the photophysical properties can be described using this model. The torsion angle (ω) along the $C_3-C_8=C_{10}-C_{12}$ chain was defined as $\omega=0°$ for the *cis*-isomer and $\omega=180°$ for the *trans*-isomer.

(a)

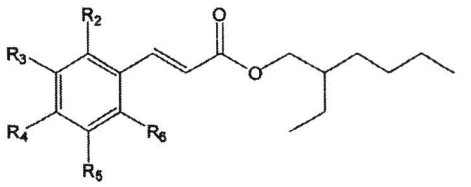

(b)

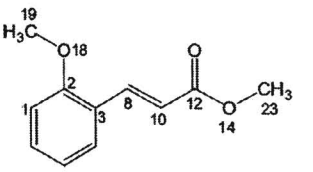

Compounds	R_2	R_3	R_4	R_5	R_6
1	OCH_3	H	H	H	H
2	H	OCH_3	H	H	H
3	H	H	OCH_3	H	H
4	OCH_3	H	OCH_3	OCH_3	H
5	OCH_3	H	OCH_3	H	OCH_3

FIG. 1. Chemical structures of (a) 2-ethylhexyl-cinnamate derivatives and (b) the calculated model compounds and atom numbering of *trans*-isomers.

The ground state (S_0) geometries were fully optimized without restricting the symmetry using the B3LYP[26,27]/6-311G(d)[28] method. The vertical excitation energies were calculated for the optimized geometries of the S_0 state using the SAC-CI method with the double-zeta basis set of the Huzinaga and Dunning plus polarization function [D95(d)].[29] To calculate the emission energy, the geometry optimization was performed for the first singlet excited (S_1) states using the CIS/D95(d) method with restricting the planar structure, except for the *cis*-**5** compound. The emission from this local minimum was observed in previous experimental work,[7] although the global minimum exists in the nonplanar structure where the torsion angle (ω) of the $C_3-C_8=C_{10}-C_{12}$ chain is around 90°. The emission energies were calculated using the SAC-CI method with the D95(d) basis sets. The SAC-CI calculations based on the CIS optimized structure have been validated in many applications for photofunctional molecules and biological compounds.[14,20–23] In addition, to investigate the energy barrier for the rotation of the methoxy group that affects the optical properties, the ground state potential energy curves along the rotation (θ) of the methoxy group with respect to the phenyl ring ($C_1-C_2-O_{18}-C_{19}$) were calculated using the B3LYP/6-311G(d) method.

In the SAC/SAC-CI calculations, the singles- and doubles-(SD)-*R* method with the direct calculation of the σ-vector, i.e., the direct SAC-CI approach[30] was used. The perturbation selection technique[31] was used to reduce the computational cost and a LevelTwo accuracy was adopted. The threshold of the linked terms for the ground state was set to $\lambda_g=5.0\times10^{-6}$. All the product terms generated by the doubles were included in the SAC calculations. For the excited states, the threshold of the linked doubles was set to

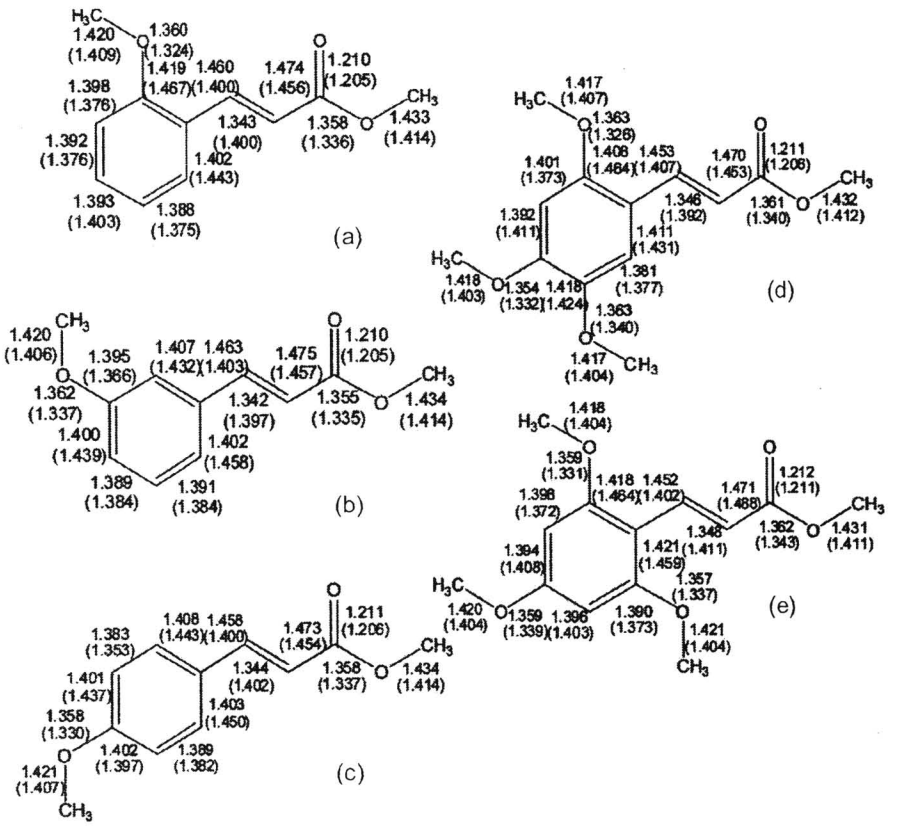

FIG. 2. A comparison of the changes in C–C and C–O bond lengths along the conjugation between the ground state and the first singlet excited state (in parentheses) of (a) *trans*-**1**, (b) *trans*-**2**, (c) *trans*-**3**, (d) *trans*-**4**, and (e) *trans*-**5** calculated using the B3LYP/6-311G(d) and CIS/D95(d) methods, respectively.

$\lambda_c = 5.0 \times 10^{-7}$. All the product terms generated by the $R_1 S_2$ and $R_2 S_2$ operators were included in the SAC-CI calculations. The SAC/SAC-CI calculations were performed using the GAUSSIAN03 suite of programs[32] with modifications for executing the direct SAC-CI method.[30]

The results of LevelTwo are usually reliable for the direct SAC-CI calculations: In the present case, the deviations to those of LevelThree were within 0.05 eV for three excited states of *para*-(**3**) methoxy substitution.

III. RESULTS AND DISCUSSION

A. Ground state and excited state geometries

The ground and first excited state geometries of the *cis*- and *trans*-isomers of *ortho*-(**1**), *meta*-(**2**), *para*-(**3**) and the 2,4,5-(4) and 2,4,6-(5) methoxy substituted compounds were investigated. The results of the *trans*-isomers are shown in Fig. 2, and those of the *cis*-isomers are given in Fig. 3. All the compounds, except for the *cis*-**5** compound, had local minima in the coplanar structure of the *cis*- and *trans*-isomers in both the S_0 and S_1 states due to π-conjugation. As shown later, in the S_0 state, the rotational energy barrier of the methoxy group is very low, although the planar structure is the most stable structure. In the S_1 state, the global minima are in the form of a nonplanar structure, but local minima exist in the planar structure. The emission was observed from this local minimum in the planar structure and, in particular, a strong emission was observed for compound **2**. The lifetime was also measured for all the compounds with regard to this emission.[7] A characteristic molecule is the *cis*-**5** compound, which has a stable nonplanar structure with the torsion angle of $\omega = 7.6°$ in the S_0 state because of steric effects. A local minimum of the *cis*-**5** compound in the S_1 state could not be obtained.

A comparison of the C–C and C–O bond lengths along the conjugation between the S_0 and S_1 state geometries of the *trans*-isomers of the methoxy substituted compounds is shown in Fig. 2. It was found that the C_1–C_2, C_3–C_8, C_{10}–C_{12}, C_{12}–O_{14}, and O_{14}–C_{23}bond lengths decrease and the length of the other bonds increases. In the S_0 state, the carbon-carbon bond alternation exists for both the single and double bonds, but this bond alternation relaxes in the S_1 state. Since the excitation is relatively localized in the central unit, the prominent changes occur in the vinylene unit. For example, in the *trans*-**1** compound, the changes in bond length are $\Delta r = +0.048$, -0.060, and $+0.057$ Å for C_2=C_3, C_3–C_8, and C_8=C_{10}, respectively, while the other changes in bond length are within 0.022 Å.

The geometry change in the excited state could be qualitatively interpreted using ESF theory. We analyzed the geometry relaxation in the S_1 state of the *trans*-**3** molecule. Based on ESF theory, the geometry change in the excited state is caused by the force acting on the nuclei due to the change in electron distribution. The molecular geometry is determined by balancing the atomic dipole, exchange (EC), and gross charge forces.[24,25] The difference in the SAC/

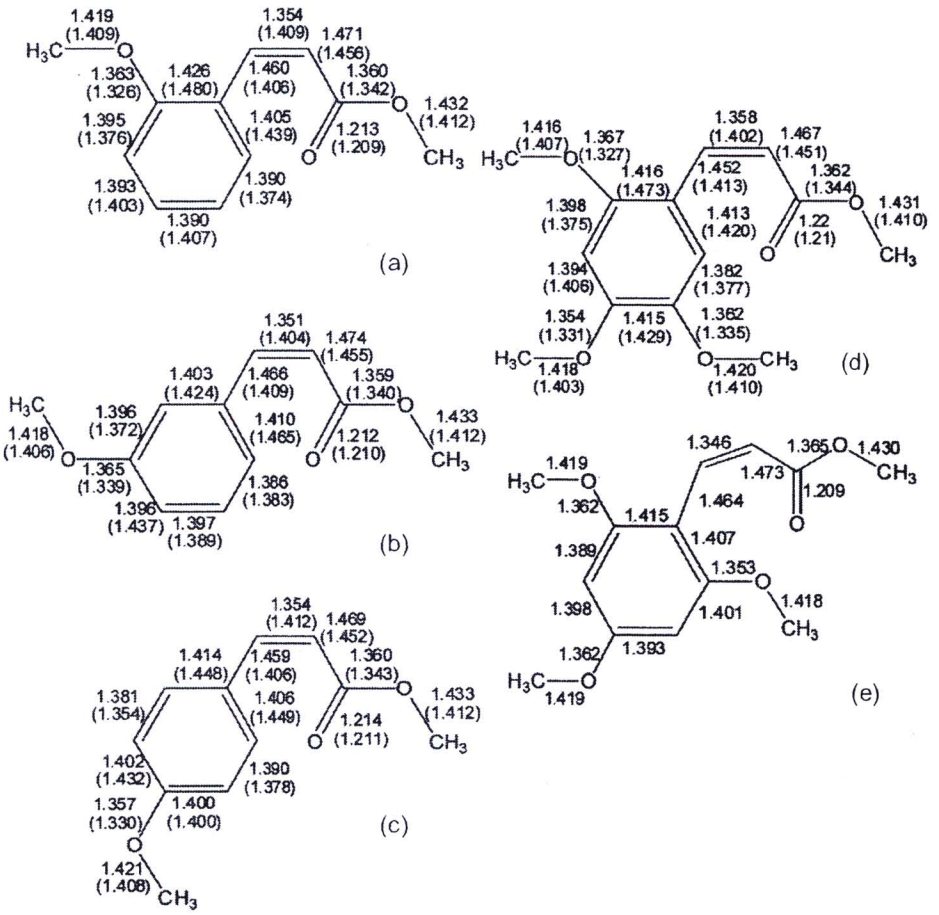

FIG. 3. A comparison of the changes in C–C and C–O bond lengths along the conjugation between the ground state and the first singlet excited state (in parentheses) of (a) *cis*-**1**, (b) *cis*-**2**, (c) *cis*-**3**, (d) *cis*-**4**, and (e) *cis*-**5** calculated using the B3LYP/6-311G(d) and CIS/D95(d) methods, respectively.

SAC-CI electron density between the S_0 and S_1 states in the ground state geometry is shown in Fig. 4. The EC force of the C=C bond decreases because of the decrease in electron density, while the EC force enhances the C–C bond. For example, the C_1–C_2, C_3–C_8, C_{10}–C_{12}, C_{12}–O_{14}, and O_{14}–C_{23} bonds shrink where the electron density increases (blue) and the C_2=C_3 and C_8=C_{10} bonds become longer where the electron density decreases (yellow). Geometry relaxation of other molecules can also be explained in the same manner.

The rotation of the methoxy group relative to the plane of the phenyl ring was investigated. The *ortho*-(*trans*-**1**), *meta*-(*trans*-**2**), and the *para*-(*trans*-**3**) monomethoxy substituted compound were examined for the C_1–C_2–O_{18}–C_{19} angle (θ) from 0° to 90° in steps of 15°. We calculated the potential energy curves with freezing other coordinates and estimated the energy barrier. The potential energy curves for this rotation are shown in Fig. 5, and these indicate that the most stable conformation was located at a angle of θ=0° for the *trans*-**1**, *trans*-**2**, and *trans*-**3** compounds. At the rotation angle of 90°, the energy barriers to the perpendicular confor-

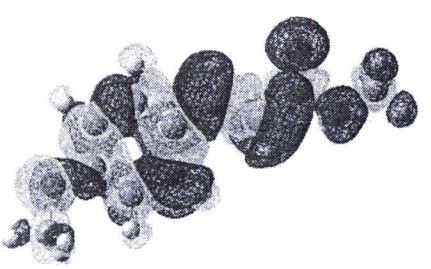

FIG. 4. Density difference maps of the *trans*-**3** of methoxy substituted molecules with a positive diffuse (blue) and a negative diffuse (yellow).

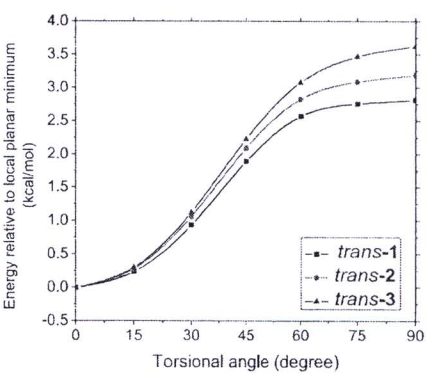

FIG. 5. Ground state potential energy curves along the rotation of the methoxy group (θ) for the *trans*-**1**, *trans*-**2**, and *trans*-**3** compounds calculated using the B3LYP/6-311G(d) method.

mation of the methoxy group for the *trans*-**1**, *trans*-**2**, and *trans*-**3** compounds were 2.8, 3.2, and 3.6 kcal/mol, respectively. This shows that the π-conjugation of the *trans*-**3** compound is slightly more effective than that of the *trans*-**1** and *trans*-**2** compounds in the planar structure. The extent of π-conjugation between the methoxy oxygen and the phenyl ring could be reflected in the C–O bond length; when the bond is shorter, the conjugation is more effective. In the *trans* compounds, the CO bond lengths are 1.360, 1.362, and 1.358 Å, for *trans*-**1**, *trans*-**2**, and *trans*-**3** compounds, respectively. In *trans*-**1**, the intramolecular C–H···O hydrogen bond interaction between the oxygen atom of the methoxy group and the hydrogen atom in the vinylene group also exists, which causes a reverse effect on the energy barrier. This low rotational energy barrier of about 1.0 kcal/mol from $\theta=0°-30°$ indicates that a wide range of nonplanar conformations is possible at room temperature. The effect of the nonplanar structure on the absorption spectra will be discussed later.

B. Absorption spectra

The absorption spectra of the *cis*- and *trans*-isomers of the five methoxy substituted cinnamates were investigated. The vertical excitation energies were calculated using the SAC-CI/D95(d) method in their ground state optimized structure. The calculated excitation energies, oscillator strength, and dipole moments are summarized in Table I, along with the experimental values observed in hexane and methanol.[7] The A' states were assigned to the $\pi\pi^*$ excited states with a large oscillator strength, while the A'' states were due to the $n\pi^*$ transition. Three low-lying excited states were found to be relevant in the energy region of the UV absorption. The higher excited states were also examined, up to around 7 eV, but as these states are located above 5 eV, they do not contribute to the important energy region for UVB absorption of 290–320 nm (4.28–3.87 eV). Compound 3 is the standard commercial product for UVB protection.

For the monomethoxy substituted compounds, the excited states that contribute to the absorption have a different character that depends on the methoxy substituted position. In the case of the ortho-(*cis*-**1** and *trans*-**1**) and *meta*-(*cis*-**2** and *trans*-**2**) compounds, the S_3 state has the highest transition probability and is characterized as being the transition from the next highest occupied molecular orbital (next HOMO) to lowest unoccupied molecular orbital (LUMO) (nH-L) transition, whereas the highest transition possibility of the *para*-(*cis*-**3** and *trans*-**3**) compounds was calculated for the $S_0 \rightarrow S_1$ transition, and the excitation character is a HOMO-LUMO (H-L) transition. The agreement with the experimental values was satisfactory. The deviations from the experimental values in peak position were within about 10 nm. For example, for the *cis*-**2** compound, the calculated values were 261 and 314 nm, compared to the experimental values of 274 (271) and 313 nm, respectively.[7] For the transition probability, the observed absorption coefficients of the *trans*-**1** compound are 13 500 and 18 100 M^{-1} cm^{-1} for the lower and higher peaks, respectively,[7] and the calculated oscillator strengths are 0.26 and 0.38 for these peaks, respectively.

The deviation from the experimental data can be attributed to the solvent effect and/or our model neglecting the side chain. The polar solvent effect is relatively small for compounds **1** and **2**, as the difference in the experimental excitation energy between hexane and methanol solutions is within 4 nm, while it is large for compound **3** at 7–19 nm.[7] The dipole moments of the ground and excited states were calculated to interpret the solvent effect qualitatively. The calculated dipole moments of the excited state were larger than that of the ground state, which causes a redshift of the peaks in a polar solvent. We also calculated the absolute values of the changes in the dipole moments from the ground state to excited states, $|\Delta\mu|=|\mu_{ES}-\mu_{GS}|$, which are shown in Table I, to examine the solvent effect before the solvent reorientation due to the excitation of cinnamates. The *cis*-isomers of compounds **1** and **2** showed changes in their dipole moments between the ground and excited states of $|\Delta\mu|=0.27$ and 2.89 D, respectively, whereas the change in dipole moment of compound **3** was around $|\Delta\mu|=4.02$ D, which also explains the observed experimental trend. However, our calculations for compounds **4** and **5** could not explain the experimental data. The *cis*- and *trans*-isomers of compound **4** show large changes in their dipole moments, around $|\Delta\mu|=5.66$ and 4.38 D, compared to the energy shifts of only 4 and 1 nm, respectively. This may be explained by the direct interaction between methanol and cinnamates.

The trimethoxy substituted compounds at the *ortho*-, *meta*-, and *para*-positions (*cis*-**4** and *trans*-**4**) show two separate peaks, and the strong lowest absorption occurs around 350 nm. However, this lowest peak is below the UVB region of interest. The *trans*-**5** compound has the S_1 state at 307 nm with a large oscillator strength of 0.64. However, this value is lower than that of the *trans*-**3** compound of 0.76 (S_1+S_2). Experimental data also show the same trend. The absorption coefficients were 24 700 and 19 900 M^{-1} cm^{-1} in methanol for the *trans*-**3** and *trans*-**5** compounds, respectively.[7] The $1A'$ and $2A'$ states were characterized as being H-L and nH-L transitions, respectively, for both compounds **4** and **5**. The *para*-methoxy substitution has an important effect in achieving a large oscillator strength of H-L transition in cinnamates. Methoxy substitution in the meta-position leads to a decrease in the oscillator strength of the H-L transition, as also seen in compound **2**. A comparison with the absorption spectrum of methyl hydroxyl cinnamate (pCA)[8] in the gas phase shows that the substitution of methoxy for OH results in changes in the oscillator strengths of the S_1 and S_2 transitions. The oscillator strength of the H-nL transition increases in methoxy substituted compound: The TD-DFT calculation predicted that the S_2 state has smaller oscillator strength in hydroxy cinammate.

Figure 6 shows the MOs relevant for the three low-lying excited states for the *trans*-**1**, *trans*-**2**, and *trans*-**3** compounds which correspond to the *cis*-**1**, *cis*-**2**, and *cis*-**3** compounds, whereas compounds **4** and **5** are shown in Fig. 7. The pattern of the MOs of the *cis*-forms is similar to that of the *trans*-ones. The HOMO, next HOMO, and LUMO are

TABLE I. Excitation energy (E_{ex}), absorption wavelength (λ_{max}), oscillator strength (f), excitation character, and dipole moment change ($|\Delta\mu|$) for the *cis*- and *trans*-isomers of methoxy substituted cinnamates calculated using the SAC-CI/D95(d) level of theory. Experimental values are cited from Ref. 7.

		SAC-CI					Experiment (nm)	
Molecule	State	E_{ex} (eV)	λ_{max} (nm)	f	Excitation character	$\|\Delta\mu\|$ (D)[a]	MeOH	Hexane
cis-**1**	XA'					(2.44)		
	$1A'$	3.83	323	0.25	0.77(H→L)	4.27	313	
	$1A''$	4.49	276	0.00	0.78(H-3→L)	4.46		
	$2A'$	4.51	275	0.34	0.72(nH→L)	0.27	271	274
trans-**1**	XA'					(2.78)		
	$1A'$	3.87	321	0.26	0.77(H→L)	3.19	325	
	$1A''$	4.23	293	0.00	0.82(H-3→L)	5.96		
	$2A'$	4.64	267	0.38	0.71(nH→L)	0.25	276	272
cis-**2**	XA'					(1.09)		
	$1A'$	3.94	314	0.04	0.76(H→L)	5.56	313	
	$1A''$	4.26	291	0.00	0.82(H-3→L)	4.35		
	$2A'$	4.74	261	0.53	0.73(nH→L)	2.89	274	271
trans-**2**	XA'					(0.50)		
	$1A'$	4.06	306	0.12	0.69(H→L)	4.89	313	
	$1A''$	4.49	276	0.00	0.80(H-3→L)	5.91		
	$2A'$	4.61	269	0.47	0.62(nH→L)	2.49	278	274
cis-**3**	XA'					(0.80)		
	$1A'$	4.13	300	0.59	0.91(H→L)	4.02	303	296
	$1A''$	4.33	286	0.00	0.83(H-3→L)	4.26		
	$2A'$	4.41	281	0.04	0.71(H→nL)	0.51		
trans-**3**	XA'					(3.66)		
	$1A'$	4.17	297	0.44	0.79(H→L)	2.18	309	290
	$2A'$	4.44	279	0.32	0.65(H→nL)	1.98		
	$1A''$	4.54	273	0.00	0.79(H-3→L)	5.95		
cis-**4**	XA'					(3.02)		
	$1A'$	3.33	372	0.36	0.89(H→L)	5.66	345	349
	$1A''$	4.30	288	0.00	0.82(H-3→L)	4.52		
	$2A'$	4.34	286	0.24	0.77(nH→L)	1.70		
trans-**4**	XA'					(3.14)		
	$1A'$	3.45	360	0.41	0.88(H→L)	4.38	349	348
	$2A'$	4.48	277	0.30	0.73(nH→L)	1.95		
	$1A''$	4.52	274	0.00	0.79(H-3→L)	6.25		
cis-**5**	XA'					(2.26)		
	$1A$	4.09	303	0.24	0.83(H→L)	4.89	305	298
	$2A$	4.35	285	0.01	0.71(nH→L)	1.86		
	$3A$	4.56	272	0.11	0.70(H-4→L)	2.00		
trans-**5**	XA'					(5.04)		
	$1A'$	4.04	307	0.64	0.88(H→L)	0.73	320	312
	$2A'$	4.27	290	0.06	0.74(nH→L)	1.99		
	$1A''$	4.57	271	0.00	0.79(H-3→L)	5.88		

[a]Values show the changes in the dipole moments from the ground to excited states ($|\Delta\mu|=|\mu_{ES}-\mu_{GS}|$) and values in parentheses are ground state dipole moment.

localized on the phenylene vinylene backbone. The methoxy substitution on the phenyl ring also has a small contribution to the π-conjugation. HOMO-3 contains the lone pairs of the C=O bond, and the $n\pi^*$ transition ($1A''$ state) causes a charge transfer from the C=O bond to the phenylene vinylene. In the HOMO and next HOMO, the vinyl double bonds form bonding orbitals, and the single bonds linking the phenyl ring with the vinyl double bond are antibonding. In the LUMO, the vinyl double bonds are antibonding and the single bonds are bonding. On the other hand, the next

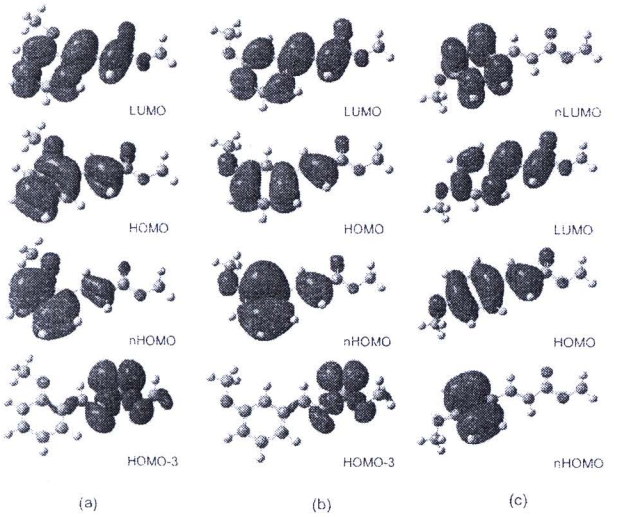

FIG. 6. MOs relevant to the low-lying excited states for (a) *ortho*-(*trans*-**1**), (b) *meta*-(*trans*-**2**), and (c) *para*-(*trans*-**3**) monomethoxy substituted molecules.

HOMO and next LUMO of the *trans*-**3** compound are localized on the benzene ring and the amplitude on vinyl double bond diminishes. These characters of MOs also explain the geometry changes in the excited states as mentioned above. The HOMO of the *trans*-**4** compound spreads over the oxygen lone pairs, which is the origin of the low-lying S_1 state in the *trans*-**4** compound.

The SAC-CI excitation spectra for the monomethoxy substituted compounds are compared to the experimental absorption spectra in Fig. 8. The experimental spectra were observed in methanol, and the polar solvent effect in terms of the energy shift was small for the *ortho*- and *meta*-substitution (less than 4 nm), and non-negligible for *para*-substitution (10–20 nm) from the experimental evidence.[7] The SAC-CI absorption spectrum of the *cis*-**3** substituted compound consists of a single absorption band, and that of the *trans*-**3** compound consists of closely separated two peaks, which is in good agreement with the experimental spectra. The absorption spectra of the *ortho*-(*cis*-**1** and *trans*-**1**) and *meta*-(*cis*-**2** and *trans*-**2**) substituted compounds consist of two distinct absorption bands. Compound **1** has two peaks with a large oscillator strength, whereas the spectra of compound **2** show a single strong peak in the higher energy region, with a shoulder on the lower energy side. These trends were well reproduced by the present SAC-CI calculations.

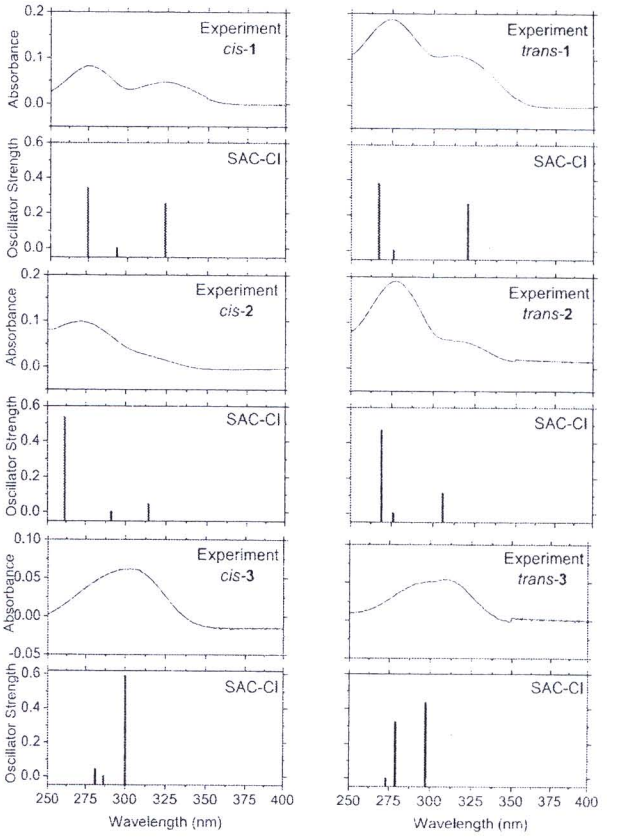

FIG. 8. SAC-CI absorption spectra of the *cis*- and *trans*-isomers of the monomethoxy substituted compounds compared with the experimental spectra in methanol (Ref. 7).

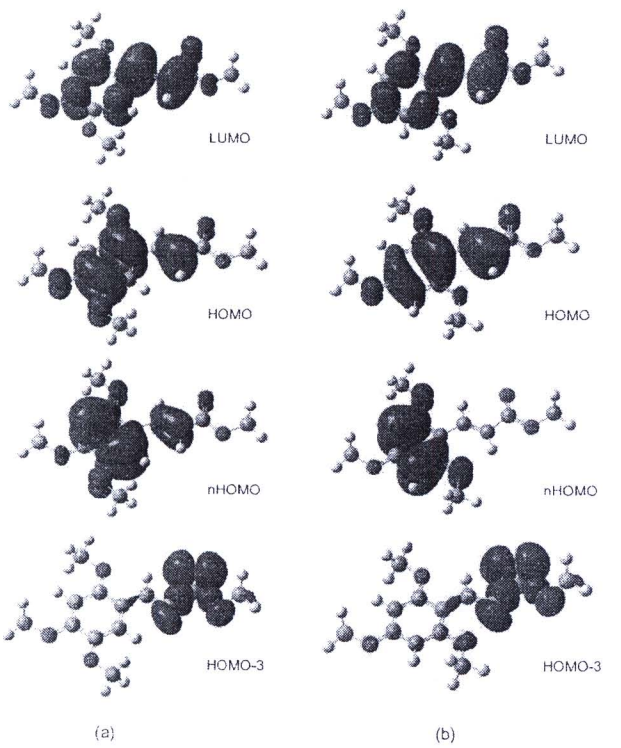

FIG. 7. MOs relevant to the low-lying excited states for (a) *trans*-**4** and (b) *trans*-**5** of the trimethoxy substituted molecules.

The SAC-CI and experimental spectra of the trimethoxy substituted compounds are compared in Fig. 9. For the trimethoxy substituted compounds, the appearance of the SAC-CI absorption spectra of the *cis*-**4** and *trans*-**4** (*ortho*-, *meta*-, and *para*-substituted) compounds was similar to those of the *cis*-**1** and *trans*-**1** (*ortho*-substituted) compounds, showing two distinct bands but with the lower peak having a higher intensity. This is in good agreement with the experimental measurements. The absorption of compound **4** in the lower energy region may be useful for blocking of the UVA

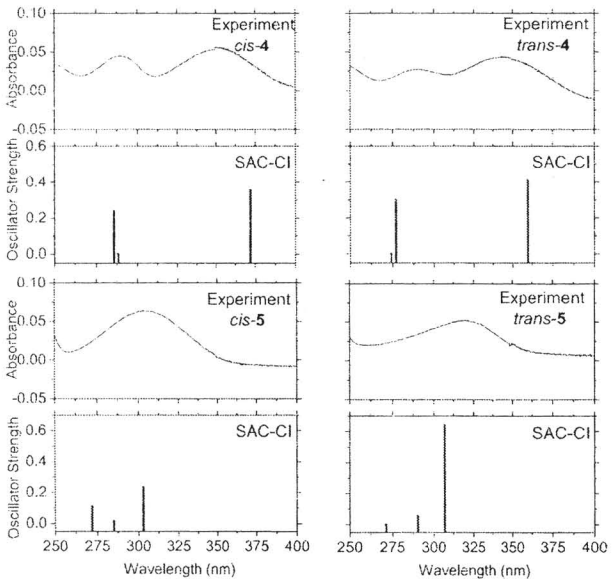

FIG. 9. SAC-CI absorption spectra of the *cis*- and *trans*-isomers of the trimethoxy substituted compounds compared to the experimental spectra in methanol (Ref. 7).

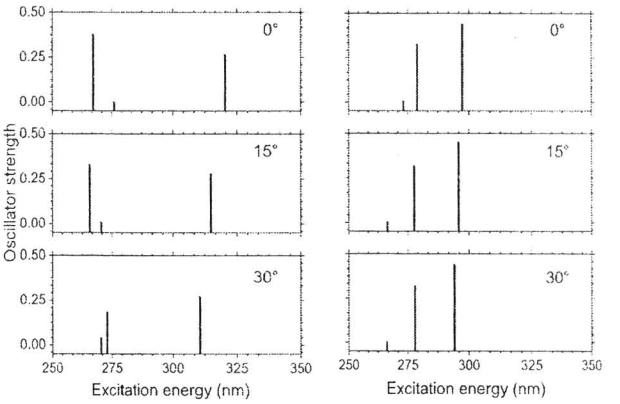

FIG. 10. Absorption spectra of the *trans*-**1** (left) and *trans*-**3** (right) compounds at a rotation angles $\theta=0°$, 15°, and 30° calculated using the SAC-CI/D95(d) method.

light. In contrast, the absorption spectra of the *cis*-**5** and *trans*-**5** (*ortho*- and *para*-substituted) compounds resemble those of the *cis*-**3** and *trans*-**3** (*para*-substituted) compounds that show a single band with a small shoulder in the higher energy region. Our theory also reproduced these experimental data.

The experimental spectra show that the absorption intensity of the *trans*-isomers is larger than that of the corresponding *cis*-isomers in all the compounds.[7] This indicates that the *trans*-isomers have better absorption efficiencies than the *cis*-isomers do. This trend was also reproduced by our SAC-CI calculations. In general, the transition dipole moment is determined by the transition dipole integrals and configuration interaction. In the present case, although the oscillator strength was distributed over two $1A'$ and $2A'$ from the configuration interaction, the difference between the *cis*- and *trans*-isomers could be attributed to the transition dipole integrals. The HOMO and LUMO orbitals of the *trans*-isomer are spread more broadly than those of the *cis*-isomer, which leads to the difference in the oscillator strength.

The ground state potential energy curve is flat along the rotation angle $\theta=0°-30°$, where the energy difference is less than 1.0 kcal/mol, and therefore, the nonplanar conformation contributes to the absorption spectra at room temperature. Therefore, we calculated the SAC-CI absorption spectra of the *trans*-**1** and *trans*-**3** compounds in the nonplanar structure. The calculated spectra with a rotation angles of $\theta=0°$, 15°, and 30° are shown in Fig. 10. For the *trans*-**1** compound, the lower energy peak shows a blueshift of about 10 nm from $\theta=0°$ to 30°, and this contributes to the shoulder observed in the higher energy region. Since the HOMO of the *trans*-**1** compound has an antiphase interaction between the benzene ring and the methoxy group, the HOMO stabilizes the nonplanar structure, and therefore, the blueshift occurs in the S_1 state of the H-L transition. The oscillator strength of the *trans*-**1** compound in the S_2 and S_3 states also interchanges along the rotation. The S_3 state is strong at $\theta=0°$, while in the distorted structure, the oscillator strength of the S_2 state increases. On the other hand, the oscillator strength of the three excited states of the *trans*-3 compound does not change much.

C. Emission spectra

The emission energies of these molecules have also been calculated using the SAC-CI method. The stable geometries of the S_1 state were located using CIS followed by the SAC-CI calculations of the vertical emission energies. The calculated emission energies, oscillator strength, and Stokes shifts are compared to the experimental data in hexane and methanol solutions in Table II. The dipole moment and excitation character of each excited state are also given in the same table.

All the compounds, except for the *cis*-**5** compound, were calculated to have the local minima in the planar structure. As discussed in Ref. 7, the global minimum of the excited state is the conical intersection where the torsion angle of the $C_3-C_8=C_{10}-C_{12}$ chain is about 90°. Molecules excited to the S_1 state with sufficient energy relax through this conical intersection beyond an energy barrier to the ground state by nonradiative decay. Nonetheless, a weak emission was observed experimentally from this local minimum of the S_1 state in the coplanar structure, in particular, for compound **2**.[7] This emission from the local minimum of the S_1 state is discussed in this work. The bond distances in the S_1 state of these molecules are shown in Figs. 2 and 3.

In general, the SAC-CI calculations reproduced the experimental trends observed in hexane solution satisfactorily. The emission energies of molecules were in the order of compounds **2** and **3** (~350 nm)<compounds **1** and **5** (~360 nm)<compound **4** (~400 nm). The deviation from the experimental values was within 10 nm, except for the *cis*-**4** compound. The transition was characterized as the HOMO-LUMO transition, and the SAC-CI coefficients are localized for this configuration. The calculated oscillator strengths were in the range of 0.41–0.68 for all the molecules, except for compound **2**. As shown in the absorption

TABLE II. Excitation energy (E_{ex}), emission wavelength (λ_{max}), oscillator strength (f), excitation character, and dipole moment for the *cis*- and *trans*-isomers of methoxy substituted cinnamates calculated using the SAC-CI/D95(d) level of theory. Experimental values are cited from Ref. 7.

		SAC-CI						Experiment (nm)	
Molecule	State	E_{ex} (eV)	λ_{max} (nm)	f	Stokes shift (eV)	Excitation character	Dipole moments (D)[a]	MeOH	Hexane
cis-**1**	$1A'$	3.43	361	0.41	0.40	0.83(H→L)	5.50(3.15)	409	361
trans-**1**	$1A'$	3.37	367	0.44	0.50	0.85(H→L)	4.68(3.32)	405	359
cis-**2**	$1A'$	3.53	351	0.10	0.41	0.76(H→L)	7.15(1.48)	410	351
trans-**2**	$1A'$	3.62	343	0.29	0.44	0.84(H→L)	5.74(1.05)	409	350
cis-**3**	$1A'$	3.55	349	0.63	0.58	0.91(H→L)	2.81(1.63)	468	354
trans-**3**	$1A'$	3.52	352	0.61	0.65	0.90(H→L)	4.89(4.37)	462	351
cis-**4**	$1A'$	2.92	424	0.44	0.41	0.90(H→L)	7.48(3.48)	461	397
trans-**4**	$1A'$	3.04	408	0.51	0.41	0.90(H→L)	7.19(4.11)	461	398
trans-**5**	$1A'$	3.43	362	0.68	0.61	0.90(H→L)	4.43(6.04)	463	358

[a]Values in parentheses show the dipole moment of the ground state (XA').

data, the S_1 state of compound **2** also had a low oscillator strength in the ground state geometry, and the transition probability is distributed to the S_3 state. The calculated Stokes shifts were 0.40–0.50 eV for compounds **1**, **2**, and **4**, and these were slightly larger, 0.58–0.65 eV for compounds **3** and **5** where the para-position is substituted by a methoxy group. This means that the excited state geometry relaxations in the S_1 state of compounds **3** and **5** are larger than those for compounds **1**, **2**, and **4**.

A redshift was observed in methanol for all the compounds.[7] To interpret this energy shift, the dipole moments of the S_0 and S_1 states calculated for the optimized geometry of the S_1 state are compared in Table II. The calculated dipole moments in the excited state are larger than those in the ground state, which explains the experimental redshift qualitatively. The redshift of the emission in methanol was marked in compounds **3** and **5** (about 100 nm), for which our calculations could not explain this effect.

The relaxation processes in the excited states are important for the UVB blocking molecules. We examined the S_1 potential energy surface of *trans*-**2** and *trans*-**3**, which mainly leads to decay by fluorescence and nonradiative decay through conical intersection, respectively.[7] Since the SAC-CI method is based on the single-reference theory, it is difficult to obtain the potential energy surface around the conical intersection. The conical intersection should be examined by the multi-reference methods such as CASSCF or multi-reference configuration interaction (MRCI), but we failed the partial optimization using the state-averaged CASSCF (4,4), (4,6), and (4,8) calculations, although CASSCF is stable around conical intersection. Therefore, we performed the SAC-CI partial optimization of the S_1 state for the torsion angles from 0° to 75° with all the other coordinates being optimized. Because of the computational limitation, the small basis sets double-zeta valence (DZV) [3s2p/2s] and restricted active space (7 occupied and 33 unoccupied MOs) were used and the perturbation selection of the operator was not performed in the SAC-CI calculations. The potential energy curves along the minimum energy path of the S_1 state are shown for *trans*-**2** and *trans*-**3** in Fig. 11. In *trans*-**2**, the energy barrier to the conical intersection was calculated to be about 5.5 kcal/mol (0.24 eV), while *trans*-**3** has a low energy barrier about 0.6 kcal/mol (0.03 eV). These calculations qualitatively explain the experimental fact that the activation energies based on the nonradiative deactive rate of *trans*-**2** and *trans*-**3** compounds were estimated to be 1.4 and 0.4 kcal/mol, respectively.[7] The ground state surface of *trans*-**3** was too steep along the torsion, for which we think the errors come from the quasidegenerate character of the states and the restricted active space.

IV. CONCLUDING REMARKS

The electronic structures and optical properties of cinnamate derivatives at five different substituted positions were investigated using the SAC-CI method. Both the *cis*- and *trans*-isomers were examined for *ortho*-, *meta*-, and *para*-monomethoxy substituted compounds and 2,4,5-(*ortho*-, *meta*-, *para*-) and 2,4,6-(*ortho*-, *para*-) trimethoxy compounds.

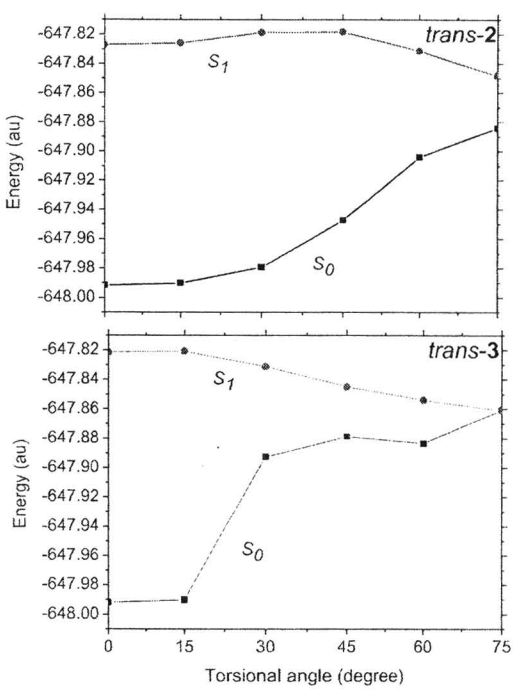

FIG. 11. The SAC-CI potential energy curves of the S_0 and S_1 states along the minimum energy path of the S_1 state are shown for *trans*-**2** and *trans*-**3**.

All compounds have a local minimum in the *cis*- and *trans*-isomers in the planar structure in both the S_0 and S_1 states, except for the 2,4,6-trimethoxy compound. The SAC-CI/D95(d) calculations reproduced the recently observed absorption and emission spectra satisfactorily, and allowed a detailed assignment and interpretation of the spectra. Three low-lying excited states were found to be relevant for the absorption in the UV blocking energy region. The calculated oscillator strengths of the *trans*-isomers were larger than all the *cis*-isomers, which is in good agreement with experimental data. In the monomethoxy compounds at the *ortho*- and *meta*-positions, the most intense peak was assigned to the transition from the nH-L, whereas in the *para*-compound it was assigned to the H-L transition. This feature was interpreted from the variation of the MOs due to the different substituted positions, and was used to explain the behavior of the excited states of the trimethoxy substituted compounds.

Our SAC-CI calculations have provided reliable results and a useful insight into the optical properties of these molecules and, therefore provide a useful tool for developing UVB blocking compounds with regard to the tuning of the photoabsorption. High absorbance, broad absorption peak with small fluorescence quantum yield, and low radiative rate are expected for superior UVB sunscreen. Nonradiative decay back to the initial ground state is also relevant. Thus, the theoretical study of the relaxation process is important to design the superior UVB blocking molecules. In the present case, both *trans*- and *cis*-forms can be generated in the course of the relaxation at around the conical intersection and *cis*-form also has absorption in the UVB region.

ACKNOWLEDGMENTS

We would like to thank Asst. Professor Fukuda and Professor Nakatsuji for the direct SAC-CI program code. We also thank the reviewers for the valuable comments. This work was supported by the Thailand Research Fund and the Commission on Higher Education (CHE) (Grant No. RTA5080005 for S.H, Grant No. MRG5180287 for S.S., and Grant No. MRG4980160 for T.K.). M.P. is grateful to the Thailand Graduate Institute of Science and Technology (TGIST) for a scholarship. M.E. was supported by the grant from the JST-CREST, Scientific Research in Priority Areas "Molecular Theory for Real Systems" from the Ministry of Education, Culture, Sports, Science and Technology of Japan (MEXT) , the Next Generation Supercomputing Project, and the Molecular-Based New Computational Science Program, NINS. The Postgraduate Education and Research Program in Petroleum, Petrochemical Technology and Advance Materials (NCE-PPAM), Center of Nanotechnology Kasetsart University, Kasetsart University Research and Development Institute (KURDI), National Nanotechnology Center (NANOTEC), Laboratory of Computational and Applied Chemistry (LCAC), Bilateral Research Cooperation (BRC), and Institute for Molecular Science (IMS) are gratefully acknowledged for partial support and research facilities. The parts of the computations were performed using Research Center for Computational Science, Okazaki, Japan.

[1] T. Monhaphol, B. Albinsson, and S. Pattanaargson, J. Pharm. Pharmacol. **59**, 279 (2007).
[2] L. Oriol, M. Pinol, J. L. Serrano, and R. M. Tejedor, J. Photochem. Photobiol., A **155**, 37 (2003).
[3] S. Pattanaargson and P. Limphong, Int. J. Cosmet. Sci. **23**, 153 (2001).
[4] H. B. Wang, B. C. Zhai, W. J. Tang, J. Y. Yu, and Q. H. Song, Chem. Phys. **333**, 229 (2007).
[5] T. S. Singh, S. Mitra, A. K. Chandra, N. Tamai, and S. Kar, J. Photochem. Photobiol., A **197**, 295 (2008).
[6] A. Chakraborty, S. Kar, and N. Guchhait, Chem. Phys. **320**, 75 (2006).
[7] T. M. Karpkird, S. Pattanaargson, and B. Albinsson, Photochem. Photobiol. Sci. **8**, 1455 (2009).
[8] M. de Groot, E. V. Gromov, H. Köppel, and W. J. Buma, J. Phys. Chem. B **112**, 4427 (2008).
[9] S. Pattanaargson, T. Munhapol, N. Hirunsupachot, and P. Luangthongaram, J. Photochem. Photobiol., A **161**, 269 (2004).
[10] G. J. Smith and I. J. Miller, J. Photochem. Photobiol., A **118**, 93 (1998).
[11] H. Nakatsuji, Chem. Phys. Lett. **59**, 362 (1978).
[12] H. Nakatsuji, Chem. Phys. Lett. **67**, 329 (1979).
[13] H. Nakatsuji, Acta Chim. Hung. **129**, 719 (1992).
[14] M. Ehara, J. Hasegawa, and H. Nakatsuji, in *Theory and Applications of Computational Chemistry: The First 40 Years*, edited by C. E. Dykstra, G. Frenking, K. S. Kim, and G. E. Scuseria (Elsevier, Oxford, 2005), p. 1099–1141.
[15] H. Nakatsuji, O. Kitao, and T. Yonezawa, J. Chem. Phys. **83**, 723 (1985).
[16] J. Wan, M. Ehara, M. Hada, and H. Nakatsuji, J. Chem. Phys. **113**, 5245 (2000).
[17] J. Wan, J. Meller, M. Hada, M. Ehara, and H. Nakatsuji, J. Chem. Phys. **113**, 7853 (2000).
[18] H. Nakatsuji, J. Hasegawa, and M. Hada, J. Chem. Phys. **104**, 2321 (1996).
[19] H. Nakatsuji, J. Hasegawa, and K. Ohkawa, Chem. Phys. Lett. **296**, 499 (1998).
[20] K. Fujimoto, J. Y. Hasegawa, S. Hayashi, S. Kato, and H. Nakatsuji, Chem. Phys. Lett. **414**, 239 (2005).
[21] N. Nakatani, J. Y. Hasegawa, and H. Nakatsuji, J. Am. Chem. Soc. **129**, 8756 (2007).
[22] P. Poolmee, M. Ehara, S. Hannongbua, and H. Nakatsuji, Polymer **46**, 6474 (2005).
[23] B. Saha, M. Ehara, and H. Nakatsuji, J. Phys. Chem. A **111**, 5473 (2007).
[24] H. Nakatsuji, J. Am. Chem. Soc. **95**, 345 (1973).
[25] H. Nakatsuji and T. Koga, in *The Force Concept in Chemistry*, edited by B. M. Deb (Van Nostrand Reinhold, New York, 1981), p. 137.
[26] A. D. Becke, Phys. Rev. A **38**, 3098 (1988).
[27] C. Lee, W. Yang, and R. G. Parr, Phys. Rev. B **37**, 785 (1988).
[28] R. Krishnan, J. S. Binkley, R. Seeger, and J. A. Pople, J. Chem. Phys. **72**, 650 (1980).
[29] T. H. Dunning, Jr. and P. J. Hay, in *Modern Theoretical Chemistry*, edited by H. F. Schaefer III (Plenum, New York, 1976), Vol. 3, p. 1.
[30] R. Fukuda and H. Nakatsuji, J. Chem. Phys. **128**, 094105 (2008).
[31] H. Nakatsuji, Chem. Phys. **75**, 425 (1983).
[32] M. J. Frisch, G. W. Trucks, H. B. Schlegel *et al.*, GAUSSIAN 03, Revision B.01, Gaussian, Inc., Pittsburgh, PA, 2003.